

Majorana multipole response: General theory and application to wallpaper groups

Shingo Kobayashi,¹ Yuki Yamazaki,² Ai Yamakage,² and Masatoshi Sato³

¹*RIKEN Center for Emergent Matter Science, Wako, Saitama 351-0198, Japan*

²*Department of Physics, Nagoya University, Nagoya 464-8602, Japan*

³*Yukawa Institute for Theoretical Physics, Kyoto University, Kyoto 606-8502, Japan*

(Dated: November 11, 2021)

Whereas identification of Cooper pair symmetry is the first and crucial step in the investigation of unconventional superconductors, only a few have been established so far because of its own difficulties. To solve this problem, we develop a theory for identification of pairing symmetry using knowledge of topological superconductivity. Establishing the multipole theory of emergent Majorana fermions in time-reversal-invariant topological superconductors, we discover a one-to-one correspondence between the electromagnetic response of Majorana fermions and Cooper pair symmetry. The emergent Majorana fermions host magnetic structures that share the same irreducible representation with Cooper pairs under crystalline symmetry. We furthermore reveal that Majorana fermions in high-spin or nonsymmorphic superconductors may exhibit magnetic octupole responses, which give a direct evidence of these exotic superconducting states. Electric responses of multiple Majorana Kramers pairs are also clarified. Our theory provides the fundamentals for identification of unconventional Cooper pairings through surface-spin-sensitive measurements as well as that for manipulation of Majorana fermions by external electromagnetic fields.

I. INTRODUCTION

Over the past decade, tremendous progress has been made in understanding of topological phases of matter. Comprehensive classifications based on the K -theory [1–17] and the symmetry-indicator [18–23] have been pushed forward to search for new topological phases enabled by crystalline symmetry. In particular, by incorporating the first-principle calculations and material databases, the symmetry-indicator method has uncovered several thousands of topologically nontrivial materials [24–29].

While these classifications can be extended to topological superconductors (TSCs) [30–35], the search for TSCs faces its own difficulties which do not exist in other topological materials: Whereas the classifications rely on Cooper pair symmetry, the identification of the latter is very difficult. In fact, in spite of a lot of effort, the exact Cooper pair symmetry has yet to be determined in many unconventional superconductors, with a few exceptions such as high- T_c cuprates. Because the typical energy scale of unconventional superconducting gaps is much smaller than that of insulating gaps, the experimental means to identify the pairing symmetry is limited. For instance, the angle-resolved photoemission spectroscopy, which is commonly used to identify topological materials, is not available, because its resolution has not reached the energy scale of the superconducting gap. Moreover, there is no established theory for the prediction of Cooper pair symmetry. The first-principle calculation, which is powerful for the prediction of topological insulators, has not been reliable yet for the calculation of unconventional pairing states. Therefore, a new principle to identify the pairing symmetry is highly desired.

In this paper, we show that Cooper pair symmetry in time-reversal invariant TSCs is directly measured by electromagnetic responses of Majorana fermions (MFs) on their surfaces. The emergent MFs appear as sur-

face zero energy Andreev bound states [36–49] and have been paid the most attention as a potential candidate for fault-tolerant qubits for topological quantum computation [50]. The increased interest in the emergent MFs offers proposals of versatile time-reversal invariant TSCs, such as superconducting doped topological insulators [51–58] and Dirac semimetals [59–66]. The MFs in time-reversal invariant TSCs commonly form Kramers pairs at zero energy, which we dub Majorana Kramers pairs (MKPs). They host the spin degrees of freedom ensured by time-reversal symmetry (TRS), which constitutes electromagnetic structures unique to the emergent MFs. The existence of electromagnetic structures provides possibility of electromagnetic responses even though the emergent MFs are electrically neutral. In addition, TSCs often host topological invariants protected by crystalline symmetry [5–7, 9, 67], and MKPs receive an additional constraint from them. The electromagnetic structures associated with MKPs turn out to acquire versatile structures and realize an anisotropic magnetic response [47, 68–79]. Such magnetic anisotropy is a salient feature of the emergent MFs, since neither electric nor magnetic responses are possible for elementary Majorana particles [80–82].

To prove the relation between electromagnetic structures and Cooper pair symmetry, we establish a general theory of electromagnetic structures of MKPs. Then, using the general theory, we exhaustively classify the electromagnetic structures under crystalline symmetry. We consider all possible minimal set of MFs located at any of the highest symmetry points on surface Brillouin zones (BZs). Our theory depends only on the irreducible representations (irreps) of MKPs and Cooper pairs, and it can calculate responses of MKPs protected by \mathbb{Z} and \mathbb{Z}_2 invariants [76, 77, 79] in a unified way. The results show that the one-to-one correspondence between irreps of magnetic couplings and those of Cooper pairs always

holds whenever only a single MKP exists. The irreps of magnetic structures are manifest in possible electromagnetic multipole responses. The emergent MFs show magnetic dipole order, but they also exhibit magnetic octupole one in special situations. There are two types of mechanisms for the magnetic octupole: (i) spin 3/2 symmetry induced magnetic octupole and (ii) nonsymmorphic symmetry induced magnetic octupole. Whereas the former one was partially discussed in our previous study [76], we here generalize it to all surface MFs with wallpaper groups. We also discover the latter mechanism of the magnetic octupole order, which is realized by MKPs protected by glide symmetry. These results indicate that the magnetic octupole responses provide a direct evidence of the exotic superconductivity in high-spin or non-symmorphic superconductors.

The above one-to-one correspondence does not hold when multiple MKPs exist on a surface. Even in this case, however, we can determine the pairing symmetry through the responses of MFs. In addition to the magnetic responses, the multiplicity of MFs enables the electric responses. One may specify Cooper pair symmetry by combining these two responses.

This paper is organized as follows. In Sec. III, we develop a general theory of electromagnetic responses of MFs in time-reversal invariant TSCs. First, we summarize relevant symmetries in Sec. III A. Then, in Sec. III B, we introduce the topological invariants for surface MFs by combining the group theoretical method with the K -theory classification. In Sec. III C, we count the minimal degeneracy of surface MFs required by crystalline symmetry. In most cases, the minimal degeneracy is the Kramers one imposed by time-reversal symmetry (TRS), but the four-fold degeneracy is required at the \bar{M} point for pgg and $p4g$. We evaluate quantum operators of MFs and determine the leading electromagnetic couplings of MFs in Secs. III D and III E. In particular, we prove that a nonzero quantum operator of a single MKP must be a magnetic operator and shares the same irrep with the gap function. (See Eq.(52).) In Secs. IV and VI, we apply the general theory to MFs protected by the wallpaper groups. Our results for a single MKP are summarized in Tables II and III. We also discuss magnetic octupole responses in high-spin and nonsymmorphic superconductors in Secs. IV B and IV C, respectively. In Sec V, we illustrate the magnetic octupole responses by using concrete models. In Sec. VI, we clarify electromagnetic structures of double MKPs realized at the \bar{M} point of pgg and $p4g$, where the additional multiplicity enables electric structures. We first point out that MFs belong to short representations for particle-hole symmetry (PHS) or chiral symmetry (CS), because of the self-antiparticle nature of MFs. Then, by constructing the short representation explicitly, we evaluate the electromagnetic responses of the double MKPs, which are summarized in Table V. In Sec. VII, we provide a summary and discuss the experimental relevance.

II. SUMMARY OF RESULTS

Our main technical accomplishment is a multipole theory of MKPs, which allows us to determine electromagnetic structure of MKPs from only crystalline symmetry and Cooper pair symmetry in bulk superconductors. As elaborated in Sec. III D, the formulae for determining the electromagnetic structures of MKPs are given by Eqs. (40) and (55): χ_g^Ω is the character of representations on MKPs for a given group $g \in G_0$ and $\chi_g^{\Omega^\pm}$ is the character of representations decomposed into electric (+) and magnetic (−) structures. Before going into the technical details, we summarize main results of the multipole theory and connections to physical systems.

Electromagnetic structures of MKPs.—Applying the formulae (40) and (55) to the wallpaper groups which are space group symmetry preserved on a surface and focusing on a minimal MKP lying at a high-symmetry point on the surface BZ, the electromagnetic structures of MKPs are exhaustively classified in Table II and III. The key findings are summarized as follows.

- For a single MKP, only a magnetic structure is allowed, and it shares the same irrep with the Cooper pair under crystalline symmetry, i.e., $\chi_g^\Omega = \chi_g^{\Omega^-} = \eta_g$ [Eq. (52)], with η_g in Eq. (4).
- A large majority of a single MKP have a magnetic dipole; namely, the response function is given by a linear function of a magnetic field, $f(\mathbf{B}) \sim \mathbf{B} \cdot \mathbf{n}$ with \mathbf{n} being specified by crystalline symmetry (see Table II and III). Systems showing the magnetic dipole response include $^3\text{He-B}$ phase [47, 69–73], superconducting doped topological insulators/semimetals [45, 48, 49], and nodal superconductors with crystalline symmetry-protected Majorana flat bands [83–87].
- A single MKP exhibits a magnetic octupole response if the surface symmetry is $p6$, $p3m1$, $p31m$, or $p6m$ and its spin is 3/2; see Fig. 1. The response function is of the order of $\mathcal{O}(|\mathbf{B}|^3)$ since the linear terms are prohibited by the crystalline symmetry. Material candidates realizing the magnetic octupole response are high-spin superconductors such as half-Hausler compounds [88–94] and antiperovskite Dirac metals [63, 64]; topological superconducting states realize MFs with spin 3/2. The magnetic octupole response in the half-Hausler compound YPtBi has been demonstrated in Ref. 76.
- A single MKP shows another magnetic octupole response if the surface symmetry is pmg or pgg (nonsymmorphic) and the MKP emerges at a high symmetry point on the surface BZ boundary; see Fig. 2. The magnetic response is again of the order of $\mathcal{O}(|\mathbf{B}|^3)$, but the expression of the response function is different from the previous one; see Secs. IV B and IV C for more discussions. The

candidates are glide symmetry-protected topological superconductors such as UCoGe [95, 96].

- A single MKP is forbidden and double MKPs are realized if the surface symmetry is pgg or $p4g$ and the MF appears at the \bar{M} point on the surface BZ. The response function of the double MKPs consists of a mixture of several irreps, including electric response; see Sec. VI and Fig. V for more details. Our multipole theory is applicable to multiple MFs and enables us to distinguish electric structures from magnetic ones in a systematic way.

Connection to physical observables.—The electromagnetic structure of MKPs represents internal degrees of freedom of MFs such as spin and orbital and thus can be measured through the coupling to external fields such as magnetic fields, strains, and so on; see Sec. III E for more discussions. In particular, a single MKP hosts only a magnetic structure, whose irrep one-to-one corresponds to that of Cooper pairs. Thus, we can determine bulk pairing symmetries from surface magnetic responses; the magnetic structures can be probed via surface-spin-sensitive measurements such as spin-resolved tunneling spectroscopy [97, 98], spin relaxation rate [69], spin susceptibility [70], thermal conductivity [99–101] under magnetic fields, and so on. For instance, the spin susceptibility is enhanced in a particular direction due to the anisotropic spin structures of the MKP [70, 84]. The anisotropy is directly linked to Cooper pair symmetry under crystalline symmetry.

III. GENERAL THEORY

A. Symmetries

Three-dimensional (3d) time-reversal invariant TSCs host helical Majorana fermions on their surfaces, which are ensured by the so-called 3d winding number [1, 39, 102, 103]. While the 3d winding number is defined only for fully-gapped TSC, its parity can be defined even for nodal superconductors [53] and ensures the existence of an odd number of MKPs. In this paper, we focus our attention on how MKPs respond to external electromagnetic fields. Obviously, electric fields only extract moderate responses from a MKP as they maintain TRS. On the other hand, magnetic fields substantially affect MKPs because the 3d winding number and its parity are ill-defined under TRS breaking external fields. However, this does not imply that MKPs are unstable under any magnetic field. In real systems, MKPs are also protected by crystalline symmetry when they are located at a high symmetry point or line in the surface BZ. In fact, crystalline symmetry provides an additional topological invariant that stabilizes MKPs. Therefore, even if the 3d winding number and its parity are ill-defined, MKPs cannot respond to magnetic fields so much as long as the crystalline symmetry for the additional topological invariant

is maintained. Namely, only magnetic fields that break the crystalline symmetry may destabilize MKPs.

First, we summarize symmetries considered in this paper. We consider space groups that are compatible with surfaces hosting MKPs. The corresponding space groups are wallpaper groups, which consist of 17 groups: $p1$, $p2$, pm , pg , cm , pmm , pmg , pgg , cmg , $p4$, $p4m$, $p4g$, $p3$, $p3m1$, $p31m$, $p6$, and $p6m$. In addition, we take into account TRS T , PHS C , and their combination, CS $\Gamma = -iTC$. These symmetries form a group G , which is decomposed into

$$G = G_0 + TG_0 + CG_0 + \Gamma G_0, \quad (1)$$

where G_0 is a wallpaper group. The group G acts on the Bogoliubov-de Gennes (BdG) Hamiltonian

$$H(\mathbf{k}) = \begin{pmatrix} h(\mathbf{k}) & \Delta(\mathbf{k}) \\ \Delta^\dagger(\mathbf{k}) & -h^T(-\mathbf{k}) \end{pmatrix}, \quad (2)$$

where $h(\mathbf{k})$ and $\Delta(\mathbf{k})$ are a normal Hamiltonian and a gap function, respectively. For $g \in G_0$, the action for the BdG Hamiltonian reads

$$\mathcal{U}_g^k H(\mathbf{k}) \mathcal{U}_g^{k\dagger} = H(g\mathbf{k}), \quad \mathcal{U}_g^k = \begin{pmatrix} U_g^k & \\ & \eta_g U_g^{-k*} \end{pmatrix}, \quad (3)$$

where U_g^k is a unitary operator obeying

$$U_g^k h(\mathbf{k}) U_g^{k\dagger} = h(g\mathbf{k}), \quad U_g^k \Delta(\mathbf{k}) U_g^{-kT} = \eta_g \Delta(g\mathbf{k}), \quad (4)$$

with a $U(1)$ factor η_g determined by the pairing symmetry of the gap function. (η_g must be ± 1 when the gap function has TRS.) For TRS T and PHS C , we have

$$\begin{aligned} \mathcal{U}_T H^*(\mathbf{k}) \mathcal{U}_T^\dagger &= H(-\mathbf{k}), \quad \mathcal{U}_T = \begin{pmatrix} U_T & \\ & U_T^* \end{pmatrix}, \\ \mathcal{U}_C H^*(\mathbf{k}) \mathcal{U}_C^\dagger &= -H(-\mathbf{k}), \quad \mathcal{U}_C = \begin{pmatrix} & 1 \\ 1 & \end{pmatrix}, \end{aligned} \quad (5)$$

where U_T is a unitary operator for TRS on the normal Hamiltonian with $U_T U_T^* = -1$. Using the complex conjugation operator K , we can also write Eq.(5) as

$$\mathcal{T} H(\mathbf{k}) \mathcal{T}^{-1} = H(-\mathbf{k}), \quad \mathcal{C} H(\mathbf{k}) \mathcal{C}^{-1} = -H(-\mathbf{k}), \quad (6)$$

with $\mathcal{T} = \mathcal{U}_T K$ and $\mathcal{C} = \mathcal{U}_C K$.

The unitary operator \mathcal{U}_g^k for $g \in G$ provides a projective representation of G ,

$$z_{g,h}^{ghk} \mathcal{U}_{gk}^k = \begin{cases} \mathcal{U}_g^{hk} \mathcal{U}_h^k & \text{if } g \text{ is unitary} \\ \mathcal{U}_g^{hk} (\mathcal{U}_h^k)^* & \text{if } g \text{ is anti-unitary} \end{cases}, \quad (7)$$

where $z_{g,h}^k$ is a $U(1)$ phase called factor system. The factor system is given as follows: Let $g = \{p|\mathbf{a}_p\}$ be an element of G_0 , where p is a point group operation and \mathbf{a}_p is a translation: $\{p|\mathbf{a}_p\}, \mathbf{x} \mapsto p\mathbf{x} + \mathbf{a}_p$. The product of $g = \{p|\mathbf{a}_p\}$ and $g' = \{p'|\mathbf{a}_{p'}\}$ reads

$$\begin{aligned} \{p|\mathbf{a}_p\} \{p'|\mathbf{a}_{p'}\} &= \{pp'|\mathbf{a}_{pp'} + \mathbf{a}_p\} \\ &= \{e|p\mathbf{a}_{p'} + \mathbf{a}_p - \mathbf{a}_{pp'}\} \{pp'|\mathbf{a}_{pp'}\}, \end{aligned} \quad (8)$$

where ε is the identity operator. Correspondingly, the factor system for $g, g' \in G_0$ is given by

$$z_{g,g'}^{\mathbf{k}} = z_{p,p'} e^{-i\mathbf{k} \cdot (p\mathbf{a}_{p'} + \mathbf{a}_p - \mathbf{a}_{pp'})}, \quad (9)$$

where $z_{p,p'} = \pm 1$ originates from the double projective representation of spin rotation in p and p' , and the exponential factor is the Bloch factor of $\{e|p\mathbf{a}_{p'} + \mathbf{a}_p - \mathbf{a}_{pp'}\}$. We also require that the subscript g of $\mathcal{U}_g^{\mathbf{k}}$ obeys the linear representation of G where T and C commute with any $g \in G$ and obey $T^2 = C^2 = \{e|\mathbf{0}\}$. Here $\{e|\mathbf{0}\}$ is the unit element. By combining this property with commutation relations in G , we can determine the factor system for other elements in G uniquely. For instance, for $g = \{p|\mathbf{a}_p\} \in G_0$, we have

$$\mathcal{U}_g^{-\mathbf{k}} \mathcal{U}_T = \mathcal{U}_T(\mathcal{U}_g^{\mathbf{k}})^*, \quad \mathcal{U}_g^{-\mathbf{k}} \mathcal{U}_C = \eta_g \mathcal{U}_C(\mathcal{U}_g^{\mathbf{k}})^*, \quad (10)$$

which lead to

$$z_{g,T}^{\mathbf{k}} = z_{T,g}^{\mathbf{k}}, \quad z_{g,C}^{\mathbf{k}} = z_{C,g}^{\mathbf{k}}, \quad (11)$$

because of $\mathcal{U}_{Tg}^{\mathbf{k}} = \mathcal{U}_{gT}^{\mathbf{k}}$ and $\mathcal{U}_{Cg}^{\mathbf{k}} = \mathcal{U}_{gC}^{\mathbf{k}}$. Furthermore, from $T^2 = -1$ and $C^2 = 1$, we have

$$z_{T,T}^{\mathbf{k}} = -1, \quad z_{C,C}^{\mathbf{k}} = 1, \quad (12)$$

since $\mathcal{U}_{T^2} = \mathcal{U}_{C^2} = \mathcal{U}_{\{e|\mathbf{0}\}}$.

B. Wigner's test and 1d topological invariants

When crystalline symmetry is taken into account, the topological classification is diversely ramified, and crystalline symmetry-protected topological phases appear [5–7, 9, 67]. Crystalline symmetry-protected topological invariants defined in low-dimensional subspaces may protect MKPs. In particular, MKPs at high symmetry points on surface BZs are supported by crystalline symmetry-protected 1d topological invariants.

To see this, let us consider a high symmetry point \mathbf{k} of G on a surface BZ, which is the projection of a high symmetry line $l_{\mathbf{k}}$ in the bulk BZ, and the little group $G^{\mathbf{k}}$ that keeps the high symmetry point \mathbf{k} (and the high symmetry line $l_{\mathbf{k}}$) invariant. The little group $G^{\mathbf{k}}$ is decomposed into

$$G^{\mathbf{k}} = G_0^{\mathbf{k}} + TG_0^{\mathbf{k}} + CG_0^{\mathbf{k}} + \Gamma G_0^{\mathbf{k}}, \quad (13)$$

where $G_0^{\mathbf{k}}$ consists of all elements in G_0 belonging to $G^{\mathbf{k}}$. On the 1d subspace $l_{\mathbf{k}}$, any element in $G_0^{\mathbf{k}}$ commutes with the BdG Hamiltonian $H(\mathbf{k})$. Thus, if we take the basis where $\mathcal{U}_g^{\mathbf{k}}$ ($g \in G_0^{\mathbf{k}}$) is decomposed into irreps of $G_0^{\mathbf{k}}$,

$$\mathcal{U}_g^{\mathbf{k}} = \oplus_{\alpha} \begin{pmatrix} U_g^{\alpha} \\ \eta_g(U_g^{\alpha})^* \end{pmatrix} \quad (14)$$

where α labels the irreps, then $H(\mathbf{k})$ on $l_{\mathbf{k}}$ is also decomposed into subsectors,

$$H(\mathbf{k}) = \oplus_{\alpha} H^{\alpha}(\mathbf{k}), \quad (15)$$

TABLE I. EAZ classes ($W_{\alpha}^T, W_{\alpha}^C, W_{\alpha}^{\Gamma}$) and associated 1d topological invariants

W_{α}^T	W_{α}^C	W_{α}^{Γ}	EAZ class	1d dim.
0	0	0	A	0
0	0	1	AIII	\mathbb{Z}
1	0	0	AI	0
1	1	1	BDI	\mathbb{Z}
0	1	0	D	\mathbb{Z}_2
-1	1	1	DIII	\mathbb{Z}_2
-1	0	0	AII	0
-1	-1	1	CII	$2\mathbb{Z}$
0	-1	0	C	0
1	-1	1	CI	0

where $H^{\alpha}(\mathbf{k})$ is a Hamiltonian belonging to the irrep α . The set of 1d Hamiltonians $H^{\alpha}(\mathbf{k})$ on $l_{\mathbf{k}}$ defines crystalline symmetry-protected 1d topological invariants.

To identify the 1d topological invariant of $H^{\alpha}(\mathbf{k})$, we employ the Wigner test [104–109]. The Wigner test specifies an Altland-Zirnbauer (AZ) symmetry class of $H^{\alpha}(\mathbf{k})$, which we call emergent AZ (EAZ) class, and determines a possible 1d topological invariant of $H^{\alpha}(\mathbf{k})$. For the Wigner test of $H^{\alpha}(\mathbf{k})$, we calculate three indices (W^T, W^C, W^{Γ}) defined as follows,

$$W_{\alpha}^T \equiv \frac{1}{|G_0^{\mathbf{k}}|} \sum_{g \in G_0^{\mathbf{k}}} z_{Tg,Tg}^{\mathbf{k}} \text{tr}[U_{(Tg)^2}^{\alpha}] = \pm 1, 0, \quad (16)$$

$$W_{\alpha}^C \equiv \frac{1}{|G_0^{\mathbf{k}}|} \sum_{g \in G_0^{\mathbf{k}}} z_{Cg,Cg}^{\mathbf{k}} \text{tr}[U_{(Cg)^2}^{\alpha}] = \pm 1, 0, \quad (17)$$

$$W_{\alpha}^{\Gamma} \equiv \frac{1}{|G_0^{\mathbf{k}}|} \sum_{g \in G_0^{\mathbf{k}}} \frac{z_{\Gamma, \Gamma^{-1}g\Gamma}^{\mathbf{k}}}{z_{g,\Gamma}^{\mathbf{k}}} \text{tr}[U_{\Gamma^{-1}g\Gamma}^{\alpha}]^* \text{tr}[U_g^{\alpha}] = 1, 0, \quad (18)$$

where $|G_0^{\mathbf{k}}|$ represents the number of elements in $G_0^{\mathbf{k}}$, and U_g^{α} is the irrep α of $\mathcal{U}_g^{\mathbf{k}}$. The indices ($W_{\alpha}^T, W_{\alpha}^C, W_{\alpha}^{\Gamma}$) indicates the presence and/or absence of TRS, PHS, and CS in $H^{\alpha}(\mathbf{k})$ and identify the EAZ class, as shown in Table I. Then, regarding $H^{\alpha}(\mathbf{k})$ on $l_{\mathbf{k}}$ as a 1d system in the EAZ class, we can specify the possible 1d topological invariant. See Appendix E also.

For instance, consider one of the highest symmetry points of $p2$. At the highest symmetry point, $G_0^{\mathbf{k}}$ is $p2$ itself, *i.e.* $G_0^{\mathbf{k}} = p2 = \{\{e|\mathbf{0}\}, \{2_z|\mathbf{0}\}\}$, where 2_z is two fold rotation around the z -axis. The irreps of $\mathcal{U}_g^{\mathbf{k}}$ ($g \in G_0^{\mathbf{k}}$) are the double-valued representations ${}^i\bar{E}$ ($i = 1, 2$), each of which corresponds to spin up and down states, respectively (we adopt the notation of irreps in the Bilbao Crystallographic Server [110]). TRS satisfies $[\{2_z|\mathbf{0}\}, T] = 0$

and $T^2 = -\{e|\mathbf{0}\}$, so it follows from Eq. (16) that

$$\begin{aligned} W_{i\bar{E}}^T &= \frac{1}{2} \left(-\text{tr}[U_{\{e|\mathbf{0}\}^2}^{i\bar{E}}] + \text{tr}[U_{\{2_z|\mathbf{0}\}^2}^{i\bar{E}}] \right) \\ &= \frac{1}{2} (-1 + 1) = 0. \end{aligned} \quad (19)$$

Similarly, we can calculate Eq. (17). It is necessary to pay attention to the commutation relation between C and $\{2_z|\mathbf{0}\}$, which depends on the irrep of the gap function. The gap function is a single-valued representation of $p2$, which is either A ($\eta_{\{2_z|\mathbf{0}\}} = 1$) or B ($\eta_{\{2_z|\mathbf{0}\}} = -1$). For the A gap function, Eq. (10) implies $[C, \{2_z|\mathbf{0}\}] = 0$, while for the B gap function, it implies $\{C, \{2_z|\mathbf{0}\}\} = 0$. Thus, Eq. (17) becomes

$$\begin{aligned} W_{i\bar{E}}^C &= \frac{1}{2} \left(\text{tr}[U_{\{e|\mathbf{0}\}^2}^{i\bar{E}}] - \eta_{\{2_z|\mathbf{0}\}} \text{tr}[U_{\{2_z|\mathbf{0}\}^2}^{i\bar{E}}] \right) \\ &= \frac{1}{2} (1 - \eta_{\{2_z|\mathbf{0}\}}) = \begin{cases} 0 & \text{for A gap function} \\ 1 & \text{for B gap function} \end{cases}. \end{aligned} \quad (20)$$

From $\Gamma = -iCT$, Eq. (18) is similarly obtained as

$$\begin{aligned} W_{i\bar{E}}^\Gamma &= \frac{1}{2} \left(|\text{tr}[U_{\{e|\mathbf{0}\}}^{i\bar{E}}]|^2 + \eta_{\{2_z|\mathbf{0}\}} |\text{tr}[U_{\{2_z|\mathbf{0}\}}^{i\bar{E}}]|^2 \right) \\ &= \frac{1}{2} (1 + \eta_{\{2_z|\mathbf{0}\}}) = \begin{cases} 1 & \text{for A gap function} \\ 0 & \text{for B gap function} \end{cases}. \end{aligned} \quad (21)$$

Therefore, the EAZ class is AIII for the A gap function and D for the B gap function, respectively.

These results are understood as follows. Because $^1\bar{E}$ and $^2\bar{E}$ are the $+i$ and $-i$ eigensectors of $\mathcal{U}_{\{2_z|\mathbf{0}\}}$, respectively, their bases are the eigenstates $|+\rangle$ and $|-\rangle$ defined by $\mathcal{U}_{\{2_z|\mathbf{0}\}}|\pm\rangle = \pm i|\pm\rangle$. For the A gap function, both \mathcal{T} and \mathcal{C} commutes with $\mathcal{U}_{\{2_z|\mathbf{0}\}}$ at the highest symmetry point. Therefore, we have

$$\mathcal{U}_{\{2_z|\mathbf{0}\}}\mathcal{T}|\pm\rangle = \mp i\mathcal{T}|\pm\rangle, \quad \mathcal{U}_{\{2_z|\mathbf{0}\}}\mathcal{C}|\pm\rangle = \mp i\mathcal{C}|\pm\rangle, \quad (22)$$

which implies that TRS and PHS exchange the eigensectors. Hence, neither $H^{^1\bar{E}}(\mathbf{k})$ nor $H^{^2\bar{E}}(\mathbf{k})$ keeps these symmetries, and they only retain the combination of \mathcal{T} and \mathcal{C} , namely CS. Thus they belong to class AIII, as was shown by the Wigner test above. A similar argument works for the B gap function. In this case, \mathcal{C} anticommutes with $\mathcal{U}_{\{2_z|\mathbf{0}\}}$ at the highest symmetry point, while \mathcal{T} commutes with $\mathcal{U}_{\{2_z|\mathbf{0}\}}$. As a result, $H^{^1\bar{E}}(\mathbf{k})$ and $H^{^2\bar{E}}(\mathbf{k})$ have PHS, and thus they belong to class D.

C. Degeneracy

Because of TRS with $T^2 = -1$, Majorana fermions at high symmetry points form Kramers pairs. For instance, in the above $p2$ case, $^1\bar{E}$ and $^2\bar{E}$ are related to each other by TRS, and thus once $H^{^1\bar{E}}(\mathbf{k})$ becomes topologically

non-trivial, so is $H^{^2\bar{E}}(\mathbf{k})$. Therefore, the resulting Majorana modes appear in a pair. In general, for a given irrep α at a high symmetry point, there are three possible realizations of a MKP; (i) a MKP formed with a different irrep $\bar{\alpha}$, (ii) a MKP formed within α , and (iii) a MKP formed with another α . In the case (i), the EAZ class of α does not have TRS, while in the latter two cases (ii) and (iii), it hosts TRS. Moreover, in the case (ii), TRS of the EAZ class is bosonic, while in the case (iii), TRS of the EAZ class is fermionic. For instance, the EAZ class at the \bar{X} point of pg with A gap function is DIII. (See Table II.) Thus a MKP at the $\bar{X} \equiv (\pi, 0)$ point is formed between two identical irreps (X_i, X_i) ($i = 1, 2$) (see Table VI).

The above result implies that if the irrep α in cases (i) and (iii) is two-dimensional, MFs at the high symmetry point exhibit four-fold degeneracy. As we will see later, such additional degeneracy occurs at the $\bar{M} \equiv (\pi, \pi)$ point of pgg and $p4g$.

D. Majorana operators

To study electromagnetic structures of MFs, we consider a general local quantum operator $\hat{\mathcal{O}}$ defined by

$$\begin{aligned} \hat{\mathcal{O}}(\mathbf{x}) &\equiv \sum_{ij} \hat{c}_i^\dagger(\mathbf{x}) O_{ij} \hat{c}_j(\mathbf{x}) \\ &= \frac{1}{2} \hat{\Psi}^\dagger(\mathbf{x}) \mathcal{O} \hat{\Psi}(\mathbf{x}) \\ &= \frac{1}{2} \hat{\Psi}^T(\mathbf{x}) \mathcal{U}_C \mathcal{O} \hat{\Psi}(\mathbf{x}) \end{aligned} \quad (23)$$

with $\hat{\Psi}_i^T(\mathbf{x}) = (\hat{c}_i(\mathbf{x}), \hat{c}_i^\dagger(\mathbf{x}))$ and

$$\mathcal{O} = \begin{pmatrix} O & 0 \\ 0 & -O^t \end{pmatrix}, \quad (24)$$

where the hermiticity of O implies $\{\mathcal{C}, \mathcal{O}\} = 0$. For instance, for $O = s_i$ with the Pauli matrices s_i , Eq. (23) represents a magnetic dipole momentum of electrons. Below, we show that nonzero $\hat{\mathcal{O}}$ s for MKPs are subject to crystalline symmetry, and they determine electromagnetic responses of MKPs.

We first perform the mode expansion to extract the contribution to $\hat{\mathcal{O}}$ from MKPs at a high symmetry point \mathbf{k} on a surface BZ. We decompose the quantum field $\hat{\Psi}(\mathbf{x})$ into MFs $|u_0^{(a)}(\mathbf{x})\rangle$ at \mathbf{k} and others:

$$\hat{\Psi}(\mathbf{x}) = \sum_a \hat{\gamma}_a |u_0^{(a)}(\mathbf{x})\rangle + \cdots, \quad (25)$$

where a labels MFs, and $\hat{\gamma}_a$ are Majorana operators. Here $\hat{\gamma}_a$ satisfies

$$\hat{\gamma}_a^\dagger = \sum_b \hat{\gamma}_b (C_\gamma)_{ba}^*, \quad \{\gamma_a, \gamma_b\} = (C_\gamma)_{ab}, \quad (26)$$

with $(C_\gamma)_{ba} \equiv \langle u_0^{(b)} | \mathcal{C} u_0^{(a)} \rangle$. (see Appendix A). Note that Eq. (26) reduces to the well-known Majorana condition $\gamma_a^\dagger = \gamma_a$ if we impose the additional constraint $|\mathcal{C} u_0^{(a)} \rangle = |u_0^{(a)} \rangle$. Substituting Eq. (25) into Eq. (23), we have

$$\hat{\mathcal{O}}_{\text{MF}}(\mathbf{x}) = \frac{1}{2} \sum_{a,b} \hat{\gamma}_a \hat{\gamma}_b \text{tr} \left[\mathcal{O} |u_0^{(b)}(\mathbf{x})\rangle \langle \mathcal{C} u_0^{(a)}(\mathbf{x})| \right], \quad (27)$$

then we separate symmetric and antisymmetric parts of Majorana operators in Eq. (27). Since $\{\gamma_a, \gamma_b\} = (C_\gamma)_{ab}$ is a constant, the symmetric part does not give a coupling between MFs and external fields, and thus only the antisymmetric part contributes to the coupling:

$$\hat{\mathcal{O}}_{\text{MF}}(\mathbf{x}) = -\frac{1}{8} \sum_{a,b} [\hat{\gamma}_a, \hat{\gamma}_b] \text{tr} \left[\mathcal{O} \rho^{(ab)}(\mathbf{x}) \right], \quad (28)$$

where $\rho^{(ab)}$ is given by

$$\rho^{(ab)}(\mathbf{x}) \equiv |u_0^{(a)}(\mathbf{x})\rangle \langle \mathcal{C} u_0^{(b)}(\mathbf{x})| - |u_0^{(b)}(\mathbf{x})\rangle \langle \mathcal{C} u_0^{(a)}(\mathbf{x})|. \quad (29)$$

Equation (28) is our main formula to examine electromagnetic structures of MKPs.

For further analysis, we employ a group theoretical approach. As we will show shortly, $\rho^{(ab)}$ is a single-valued representation of $G_0^{\mathbf{k}}$ under the action $\rho^{(ab)} \mapsto \mathcal{U}_g^{\mathbf{k}} \rho^{(ab)} \mathcal{U}_g^{\mathbf{k}\dagger}$ for $g \in G_0^{\mathbf{k}}$. It is decomposed into irreps as

$$\rho^{(ab)} = \sum_{Ai} \rho_i^{(A)}, \quad (30)$$

where $\rho^{(A)}$ is a single-valued irrep of $G_0^{\mathbf{k}}$ with the transformation law

$$\mathcal{U}_g^{\mathbf{k}} \rho_i^{(A)} \mathcal{U}_g^{\mathbf{k}\dagger} = \sum_j \rho_j^{(A)} [\mathcal{D}_g^A]_{ji}. \quad (31)$$

Here \mathcal{D}_g^A is a real orthogonal matrix. We can also decompose \mathcal{O} as

$$\mathcal{O} = \sum_{Ai} \mathcal{O}_i^{(A)}, \quad (32)$$

where $\mathcal{O}_i^{(A)}$ is an operator belonging to a single-valued irrep of $G_0^{\mathbf{k}}$,

$$\mathcal{U}_g^{\mathbf{k}} \mathcal{O}_i^{(A)} \mathcal{U}_g^{\mathbf{k}\dagger} = \sum_j \mathcal{O}_j^{(A)} [\mathcal{D}_g^A]_{ji}. \quad (33)$$

By substituting Eqs. (30) and (32) into Eq. (28), the trace part is recast into

$$\begin{aligned} & \sum_{A,B} \text{tr} \left[\mathcal{O}_i^{(A)} \rho_j^{(B)} \right] \\ &= \frac{1}{|G_0^{\mathbf{k}}|} \sum_{A,B,g \in G_0^{\mathbf{k}}} \text{tr} \left[\mathcal{U}_g^{\mathbf{k}} \mathcal{O}_i^{(A)} \mathcal{U}_g^{\mathbf{k}\dagger} \mathcal{U}_g^{\mathbf{k}} \rho_j^{(B)} \mathcal{U}_g^{\mathbf{k}\dagger} \right] \\ &= \frac{1}{|G_0^{\mathbf{k}}|} \sum_{A,B,k,l,g \in G_0^{\mathbf{k}}} \text{tr} \left[\mathcal{O}_k^{(A)} \rho_l^{(B)} \right] [\mathcal{D}_g^A]_{ki} [\mathcal{D}_g^B]_{lj} \\ &= \sum_{A,B,l} \frac{1}{d_A} \text{tr} \left[\mathcal{O}_l^{(A)} \rho_l^{(B)} \right] \delta_{ij} \delta_{AB}. \end{aligned} \quad (34)$$

where we have used the orthogonality of irreps:

$$\sum_{g \in G_0^{\mathbf{k}}} [\mathcal{D}_g^A]_{ki} [\mathcal{D}_g^B]_{lj} = \frac{|G_0^{\mathbf{k}}|}{d_A} \delta_{AB} \delta_{ij} \delta_{kl}, \quad (35)$$

with d_A the dimension of \mathcal{D}_g^A . Therefore, $\hat{\mathcal{O}}_{\text{MF}}$ in Eq.(28) is nonzero only when \mathcal{O} shares the same irrep as $\rho^{(ab)}$. In other words, the representation of $\rho^{(ab)}$ determines possible \mathcal{O} for MKPs.

Now we explain how to identify the representation of $\rho^{(ab)}$. A MF $|u_0^{(a)} \rangle$ at a high symmetry point \mathbf{k} is a zero mode of $H(\mathbf{k})$ on the 1d subspace $l_{\mathbf{k}}$. (More specifically, $|u_0^{(a)} \rangle$ is a zero mode of $H^\alpha(\mathbf{k})$ on $l_{\mathbf{k}}$.) Since $\mathcal{U}_g^{\mathbf{k}}$ ($g \in G_0^{\mathbf{k}}$) commutes with $H(\mathbf{k})$ on $l_{\mathbf{k}}$, $\mathcal{U}_g^{\mathbf{k}} |u_0^{(a)} \rangle$ is also a zero mode, which implies the relation

$$\mathcal{U}_g^{\mathbf{k}} |u_0^{(a)} \rangle = \sum_b |u_0^{(b)} \rangle [U_{g,\gamma}]_{ba}, \quad (36)$$

with $[U_{g,\gamma}]_{ab} \equiv \langle u_0^{(a)} | \mathcal{U}_g^{\mathbf{k}} |u_0^{(b)} \rangle$. Here $U_{g,\gamma}$ obeys the same multiplication law as $\mathcal{U}_g^{\mathbf{k}}$, and thus it is a double-valued projective representation of $G_0^{\mathbf{k}}$ with the same factor system as $\mathcal{U}_g^{\mathbf{k}}$. Similarly, the group action on $|\mathcal{C} u_0^{(a)} \rangle$ is given by

$$\begin{aligned} \mathcal{U}_g^{\mathbf{k}} |\mathcal{C} u_0^{(a)} \rangle &= \eta_g \mathcal{C} \mathcal{U}_g^{\mathbf{k}} |u_0^{(a)} \rangle \\ &= \sum_b \eta_g |\mathcal{C} u_0^{(b)} \rangle (U_{g,\gamma})_{ba}^*, \end{aligned} \quad (37)$$

where we have used the relation $\mathcal{U}_g^{\mathbf{k}} \mathcal{C} = \eta_g \mathcal{C} (\mathcal{U}_g^{\mathbf{k}})^*$ with $\mathcal{U}_g^{\mathbf{k}} = \mathcal{U}_g^{-\mathbf{k}}$ at a high symmetry point \mathbf{k} . Therefore, $\rho^{(ab)}$ is transformed as an anti-symmetric product representation of $G_0^{\mathbf{k}}$ under the action $\rho^{(ab)} \mapsto \mathcal{U}_g^{\mathbf{k}} \rho^{(ab)} \mathcal{U}_g^{\mathbf{k}\dagger}$ for $g \in G_0^{\mathbf{k}}$,

$$\begin{aligned} \mathcal{U}_g^{\mathbf{k}} \rho^{(ab)} \mathcal{U}_g^{\mathbf{k}\dagger} &= \sum_{c,d} \rho^{(cd)} \eta_g [U_{g,\gamma}]_{ca} [U_{g,\gamma}]_{db} \\ &\equiv \sum_{c,d} \rho^{(cd)} [\Omega_g]_{(cd)(ab)}, \end{aligned} \quad (38)$$

where Ω_g is given by

$$[\Omega_g]_{(cd)(ab)} = \frac{\eta_g}{2} \left([U_{g,\gamma}]_{ca} [U_{g,\gamma}]_{db} - [U_{g,\gamma}]_{da} [U_{g,\gamma}]_{cb} \right). \quad (39)$$

Since the left hand side of Eq.(38) does not change the sign when $\mathcal{U}_g^{\mathbf{k}} \mapsto -\mathcal{U}_g^{\mathbf{k}}$, the anti-symmetric product representation is a single-valued representation of $G_0^{\mathbf{k}}$.

On the basis of the standard group theory, we can perform the irreducible decomposition of $\rho^{(ab)}$ by calculating the character of Ω_g . By taking the trace of Ω_g , the character of the product representation is given by

$$\chi_g^\Omega = \frac{\eta_g}{2} \left((\text{tr} [U_{g,\gamma}])^2 - \text{tr} [(U_{g,\gamma})^2] \right). \quad (40)$$

The right hand side of Eq.(40) is evaluated as follows. In general, MFs at \mathbf{k} consist of a set of irreps; when a MF $|u_0^{(a)}\rangle$ originates from $H^\alpha(\mathbf{k})$ on $l_{\mathbf{k}}$, it is the same irrep α as $H^\alpha(\mathbf{k})$. Correspondingly, $U_{g,\gamma}$ is decomposed into

$$U_{g,\gamma} = \oplus_\alpha U_g^\alpha, \quad (41)$$

and thus we have

$$\chi_g^\Omega = \frac{\eta_g}{2} \left(\left(\sum_\alpha \text{tr} [U_g^\alpha] \right)^2 - \sum_\alpha \text{tr} [(U_g^\alpha)^2] \right). \quad (42)$$

The right hand side of Eq.(42) can be easily calculated by the character table of irrep α , without referring to the explicit form of $U_{g,\gamma}$. Finally, comparing χ_g^Ω with the characters of the single-valued irreps of $G_0^{\mathbf{k}}$, we obtain the irreducible decomposition of $\rho^{(ab)}$. In Sec. IV, we apply this method to MKPs at the highest symmetry points of all the wallpaper groups.

The distinction between electric and magnetic structures of MKPs can be done by TRS. Using TRS, \mathcal{O} and $\rho^{(ab)}$ are decomposed as

$$\mathcal{O} \equiv \mathcal{O}_+ + \mathcal{O}_-, \quad \rho^{(ab)} \equiv \rho_+^{(ab)} + \rho_-^{(ab)}, \quad (43)$$

with

$$\mathcal{O}_\pm = \frac{\mathcal{O} \pm \mathcal{T}\mathcal{O}^\dagger\mathcal{T}^{-1}}{2}, \quad \rho_\pm^{(ab)} = \frac{\rho^{(ab)} \pm \mathcal{T}\rho^{(ab)\dagger}\mathcal{T}^{-1}}{2}, \quad (44)$$

where \mathcal{O}_\pm and $\rho_\pm^{(ab)}$ satisfy

$$\mathcal{T}\mathcal{O}_\pm^\dagger\mathcal{T}^{-1} = \pm\mathcal{O}_\pm, \quad \mathcal{T}\rho_\pm^{(ab)\dagger}\mathcal{T}^{-1} = \pm\rho_\pm^{(ab)}. \quad (45)$$

Since \mathcal{O} is hermitian, the \mathcal{O}_\pm component of \mathcal{O} is nothing but the even/odd parity component of \mathcal{O} under TRS. For TRS, it holds that

$$\begin{aligned} \text{tr} [\mathcal{O}\rho^{(ab)}] &= \text{tr} [\mathcal{T}(\mathcal{O}\rho^{(ab)})^\dagger\mathcal{T}^{-1}] \\ &= \text{tr} [\mathcal{T}\rho^{(ab)\dagger}\mathcal{T}^{-1}\mathcal{T}\mathcal{O}^\dagger\mathcal{T}^{-1}] \\ &= \text{tr} [\mathcal{T}\mathcal{O}^\dagger\mathcal{T}^{-1}\mathcal{T}\rho^{(ab)\dagger}\mathcal{T}^{-1}], \end{aligned} \quad (46)$$

and thus we obtain

$$\text{tr} [\mathcal{O}_+\rho_-^{(ab)}] = \text{tr} [\mathcal{O}_-\rho_+^{(ab)}] = 0. \quad (47)$$

Therefore, the trace part of Eq.(28) is given by

$$\text{tr} [\mathcal{O}\rho^{(ab)}] = \text{tr} [\mathcal{O}_+\rho_+^{(ab)}] + \text{tr} [\mathcal{O}_-\rho_-^{(ab)}]. \quad (48)$$

As we will show in Sec.III E, the \mathcal{O}_+ (\mathcal{O}_-) component gives the primary coupling to electric (magnetic) fields because an electric (magnetic) field is even (odd) under TRS. Hence, Eq.(48) means that the leading coupling of

MKPs to electric (magnetic) fields is determined by $\rho_+^{(ab)}$ ($\rho_-^{(ab)}$).

When the system hosts only a single MKP, we have additional simplification on $\rho^{(ab)}$. In this case, $\rho^{(ab)}$ consists of a single component $\rho^{(12)}$ since only two Majorana zero modes exist. We find that this single component satisfies

$$\mathcal{T}\rho^{(12)\dagger}\mathcal{T} = -\rho^{(12)}, \quad (49)$$

as is shown in the following. Because the two Majorana zero modes $|u_0^{(a)}\rangle$ ($a = 1, 2$) are related by TRS, we can rewrite $\rho^{(12)}$ as

$$\rho^{(12)} = |u_0^{(1)}\rangle\langle\mathcal{C}\mathcal{T}u_0^{(1)}| - |\mathcal{T}u_0^{(1)}\rangle\langle\mathcal{C}u_0^{(1)}|, \quad (50)$$

which leads to

$$\mathcal{T}\rho^{(12)\dagger}\mathcal{T}^{-1} = -|\mathcal{C}u_0^{(1)}\rangle\langle\mathcal{T}u_0^{(1)}| + |\mathcal{T}\mathcal{C}u_0^{(1)}\rangle\langle u_0^{(1)}|. \quad (51)$$

Furthermore, when $|u_0^{(1)}\rangle$ is protected by \mathbb{Z}_2 (\mathbb{Z}), we have $|\mathcal{C}u_0^{(1)}\rangle = |u_0^{(1)}\rangle$ ($\Gamma|u_0^{(1)}\rangle = \lambda|u_0^{(1)}\rangle$ with $\Gamma = -i\mathcal{TC}$ and $\lambda = \pm 1$). In either case, these relations give the right hand side of Eq.(51) as $-\rho^{(12)}$, and thus we obtain Eq.(49). Equation (49) implies that $\rho^{(12)} = \rho_-^{(12)}$ and thus only \mathcal{O}_- can couple to a single MKP. Thus a magnetic field gives the primary coupling to a MKP. (See also Sec. III E). We also find that the single component $\rho^{(12)}$ and the gap function share the same irrep in this case. This property follows from that $U_{g,\gamma}$ for a single MKP is given by a rotation matrix of a spin $J/2$ fermion. Since the antisymmetric product of spin $J/2$ fermions is spin-singlet, χ_g^Ω in Eq. (40) is readily calculated as

$$\chi_g^\Omega = \eta_g. \quad (52)$$

We also confirm this relation for all single MKP cases in Tables II and III in Sec. IV. Equation (52) implies that the representation of $\rho^{(12)}$ coincides with that of the gap function.

If the system hosts more than a single MKP, both $\rho_+^{(ab)}$ and $\rho_-^{(ab)}$ can be nonzero and they can have more different irreps than the gap function. As is shown in Appendix B, $\rho_\pm^{(ab)}$ is transformed as

$$\mathcal{U}_g^{\mathbf{k}}\rho_\pm^{(ab)}\mathcal{U}_g^{\mathbf{k}\dagger} \equiv \sum_{cd} \rho_\pm^{(cd)}[\Omega_g^\pm]_{(cd)(ab)}, \quad (53)$$

where Ω_g^\pm is given by

$$\begin{aligned} &[\Omega_g^\pm]_{(cd)(ab)} \\ &= \frac{\eta_g}{4} \left([U_{g,\gamma}]_{ca}[U_{g,\gamma}]_{db} - [U_{g,\gamma}]_{da}[U_{g,\gamma}]_{cb} \right) \\ &\pm \frac{\eta_g}{4} \left([\Gamma_\gamma U_{g,\gamma}]_{ca}[\Gamma_\gamma U_{g,\gamma}]_{db} - [\Gamma_\gamma U_{g,\gamma}]_{da}[\Gamma_\gamma U_{g,\gamma}]_{cb} \right). \end{aligned} \quad (54)$$

with $[\Gamma_\gamma]_{ab} \equiv \langle u_0^{(a)}|\Gamma|u_0^{(b)}\rangle$. By taking the trace of Ω_g^\pm , the character of the representation reads

$$\begin{aligned} \chi_g^{\Omega^\pm} &= \frac{\eta_g}{4} \left((\text{tr}[(U_{g,\gamma})^2] - \text{tr}[(U_{g,\gamma})^2]) \right. \\ &\quad \left. \pm \frac{\eta_g}{4} ((\text{tr}[\Gamma_\gamma U_{g,\gamma})^2] - \text{tr}[(\Gamma_\gamma U_{g,\gamma})^2]) \right). \end{aligned} \quad (55)$$

From $\chi_g^{\Omega^\pm}$, we can identify the irreps of $\rho_\pm^{(ab)}$.

E. electric and magnetic couplings of MKPs

The presence of electric or magnetic fields may induce low energy couplings between these external fields and MKPs. Here we will explain how to determine such couplings by symmetry.

First, we consider possible magnetic couplings of MKPs induced by a magnetic field \mathbf{B} . A magnetic field \mathbf{B} induces an effective coupling \hat{H}_m between the quantum field $\Psi(\mathbf{x})$ and \mathbf{B} . In the low energy limit, \hat{H}_m does not contain any derivatives of $\Psi(\mathbf{x})$ and \mathbf{B} in the low energy limit, and thus it can be written as

$$\hat{H}_m = \int d\mathbf{x} g(\mathbf{B}) \hat{\mathcal{O}}(\mathbf{x}), \quad (56)$$

where $g(\mathbf{B})$ is a real function of \mathbf{B} , and $\hat{\mathcal{O}}$ is a local quantum operator in the form of Eq.(23). [111] Hence, the coupling between MKPs and the magnetic field is given by

$$\hat{H}_m = \int d\mathbf{x} g(\mathbf{B}) \hat{\mathcal{O}}_{\text{MF}}(\mathbf{x}), \quad (57)$$

with $\hat{\mathcal{O}}_{\text{MF}}$ in Eq.(28).

Possible $g(\mathbf{B})$ and $\hat{\mathcal{O}}_{\text{MF}}$ are subject to symmetry. In general, a magnetic field breaks (a part of) symmetry of the system. However, if one applies the symmetry operation to the magnetic field as well as the quantum operator $\hat{\Psi}$, the whole system recovers the symmetry, and thus \hat{H}_m should be invariant under this symmetry operation.

Under TRS, $g(\mathbf{B})$ and $\hat{\mathcal{O}}_{\text{MF}}$ are transformed as

$$g(\mathbf{B}) \rightarrow g(-\mathbf{B}), \quad (58)$$

and

$$\begin{aligned} \hat{\mathcal{O}}_{\text{MF}} &\rightarrow -\frac{1}{8} \sum_{a,b} [\hat{\gamma}_a, \hat{\gamma}_b] \text{tr}[\mathcal{U}_T^\dagger \rho^{(ab)} \mathcal{U}_T \mathcal{O}^*] \\ &= -\frac{1}{8} \sum_{a,b} [\hat{\gamma}_a, \hat{\gamma}_b] \text{tr}[\rho^{(ab)} \mathcal{T} \mathcal{O} \mathcal{T}^{-1}]. \end{aligned} \quad (59)$$

Therefore, if we decompose $g(\mathbf{B})$ and $\hat{\mathcal{O}}_{\text{MF}}$ as

$$\begin{aligned} g(\mathbf{B}) &= g_+(\mathbf{B}) + g_-(\mathbf{B}), \\ \hat{\mathcal{O}}_{\text{MF}} &= \hat{\mathcal{O}}_{\text{MF}+} + \hat{\mathcal{O}}_{\text{MF}-}, \end{aligned} \quad (60)$$

where $g_+(\mathbf{B})$ ($g_-(\mathbf{B})$) is an even (odd) function of \mathbf{B} , and $\hat{\mathcal{O}}_{\text{MF}\pm}$ is given by

$$\hat{\mathcal{O}}_{\text{MF}\pm} = -\frac{1}{8} \sum_{a,b} [\hat{\gamma}_a, \hat{\gamma}_b] \text{tr}[\rho_\pm^{(ab)} \mathcal{O}_\pm], \quad (61)$$

then TRS leads to

$$g_+(\mathbf{B}) \hat{\mathcal{O}}_{\text{MF}-} = g_-(\mathbf{B}) \hat{\mathcal{O}}_{\text{MF}+} = 0. \quad (62)$$

Thus, we have

$$\hat{H}_m = \int d\mathbf{x} \left(g_+(\mathbf{B}) \hat{\mathcal{O}}_{\text{MF}+}(\mathbf{x}) + g_-(\mathbf{B}) \hat{\mathcal{O}}_{\text{MF}-}(\mathbf{x}) \right). \quad (63)$$

A further constraint is obtained by crystalline symmetry. For $g = \{p|\mathbf{a}_p\} \in G_0^k$, $g_\pm(\mathbf{B})$ and $\hat{\mathcal{O}}_{\text{MF}\pm}$ are transformed as

$$g_\pm(\mathbf{B}) \rightarrow g_\pm((\det p)p\mathbf{B}), \quad (64)$$

$$\hat{\mathcal{O}}_{\text{MF}\pm} \rightarrow -\frac{1}{8} \sum_{a,b} [\hat{\gamma}_a, \hat{\gamma}_b] \text{tr}[\mathcal{U}_g^{k\dagger} \rho_\pm^{(ab)} \mathcal{U}_g^k \mathcal{O}_\pm]. \quad (65)$$

In order that \hat{H}_m is invariant under G_0^k , $g_+(\mathbf{B})$ ($g_-(\mathbf{B})$) and $\hat{\mathcal{O}}_{\text{MF}+}$ ($\hat{\mathcal{O}}_{\text{MF}-}$) should be the same irrep under the transformation in Eqs.(64) and (65).

In a similar manner, we can obtain possible electric couplings of MKPs induced by an electric (polarization) field \mathbf{E} . TRS requires that the electric couplings should have the following form

$$\hat{H}_e = \int d\mathbf{x} f(\mathbf{E}) \hat{\mathcal{O}}_{\text{MF}+}(\mathbf{x}), \quad (66)$$

since \mathbf{E} is invariant under TRS. Furthermore, $g(\mathbf{E})$ and $\hat{\mathcal{O}}_{\text{MF}+}(\mathbf{x})$ should be the same irrep under crystalline symmetry defined by $f(\mathbf{E}) \rightarrow f(p\mathbf{E})$ and Eq.(65). We note that though applying an electric field to superconductors is difficult, electric responses can be observed via a distortion of the crystal.

As discussed in Sec.III D, for a single MKP, only $\hat{\mathcal{O}}_{\text{MF}-}$ is nonzero. Therefore, a single MKP may host only the magnetic coupling. This result is consistent with the fact that TRS protects a single MKP and a time-reversal breaking magnetic field is necessary to gap it out. We need more than a single MKP to obtain the electric coupling.

IV. APPLICATION TO THE WALLPAPER GROUPS

A. Majorana multipole response

We now apply the general theory developed in the previous section to MKPs protected by wallpaper groups. We consider the minimal set of MKPs positioned at each of the highest symmetry points in the surface BZ where the little group G_0^k is G_0 itself. The minimal MKPs are systematically determined from the Wigner's test for TRS. As discussed in Sec.III C, when $W_\alpha^T = 1(-1)$, a Kramers pair is formed in a single (a pair of) α , while when $W_\alpha^T = 0$, a Kramers pair is formed between different irreps [105]. The resultant minimal MKPs are listed in Tables II and III. In most cases, the minimal set is a single MKP, and thus $\rho^{(ab)}$ consists of a single component $\rho_-^{(12)}$. As is shown in Sec.III D, the irrep of $\rho_-^{(12)}$

TABLE II. EAZ symmetry classes, irreps of $\rho_-^{(ab)}$ and magnetic responses for single MKPs for 2d point groups. The first row in each table shows the wallpaper groups, irreps of MFs, and the effective spin of MFs, where groups in parentheses represent the Schoenflies notations. For each table, the first, second, third, fourth, and fifth columns show irreps of gap functions, the emergent Altland Zirnbauer classes, the 1d invariants, irreps of $\rho_-^{(ab)}$, and the leading term of g_- , respectively. Here, “IR” stands for irreps and we adopt the notation of irreps in the Bilbao Crystallographic Server [110]. Note that irreps of MFs are double-valued irreps and irreps of Δ and \mathcal{O} are single-valued irreps.

$p1 (C_1), \bar{A}, \text{spin } 1/2$					$p2 (C_2), (^1\bar{E}, ^2\bar{E}), \text{spin } 1/2$				
IR of Δ	EAZ	1dim.	IR of $\rho_-^{(12)}$	Magetic multipole g_-	IR of Δ	EAZ	1dim.	IR of $\rho_-^{(12)}$	Magetic multipole g_-
A	DIII	\mathbb{Z}_2	A	B_x, B_y, B_z	A	AIII	\mathbb{Z}	A	B_z
					B	D	\mathbb{Z}_2	B	B_x, B_y
$p3 (C_3), (^1\bar{E}, ^2\bar{E}), \text{spin } 1/2$					$p3 (C_3), \bar{E}, \text{spin } 3/2$				
IR of Δ	EAZ	1dim.	IR of $\rho_-^{(12)}$	Magetic multipole g_-	IR of Δ	EAZ	1dim.	IR of $\rho_-^{(12)}$	Magetic multipole g_-
A	AIII	\mathbb{Z}	A	B_z	A	DIII	\mathbb{Z}_2	A	B_z
$p4 (C_4), (^1\bar{E}_1, ^2\bar{E}_1) \text{ or } (^1\bar{E}_2, ^2\bar{E}_2), \text{spin } 1/2 \text{ or } 3/2$					$p6 (C_6), (^1\bar{E}_2, ^2\bar{E}_2) \text{ or } (^1\bar{E}_3, ^2\bar{E}_3), \text{spin } 1/2 \text{ or } 5/2$				
IR of Δ	EAZ	1dim.	IR of $\rho_-^{(12)}$	Magetic multipole g_-	IR of Δ	EAZ	1dim.	IR of $\rho_-^{(12)}$	Magetic multipole g_-
A	AIII	\mathbb{Z}	A	B_z	A	AIII	\mathbb{Z}	A	B_z
B	A	0	—	—	B	A	0	—	—
$p6 (C_6), (^1\bar{E}_1, ^2\bar{E}_1), \text{spin } 3/2$					$pm (C_s), (^1\bar{E}, ^2\bar{E}), \text{spin } 1/2$				
IR of Δ	EAZ	1dim.	IR of $\rho_-^{(12)}$	Magetic multipole g_-	IR of Δ	EAZ	1dim.	IR of $\rho_-^{(12)}$	Magetic multipole g_-
A	AIII	\mathbb{Z}	A	B_z	A	AIII	\mathbb{Z}	A	B_z
B	D	\mathbb{Z}_2	B	$B_x^2 - 3B_xB_y^2, B_y^3 - 3B_yB_x^2$	B	D	\mathbb{Z}_2	B	B_x, B_y
$pmm (C_{2v}), \bar{E}, \text{spin } 1/2$					$p31m, p3m1 (C_{3v}), \bar{E}_1, \text{spin } 1/2$				
IR of Δ	EAZ	1dim.	IR of $\rho_-^{(12)}$	Magetic multipole g_-	IR of Δ	EAZ	1dim.	IR of $\rho_-^{(12)}$	Magetic multipole g_-
A ₁	CI	0	—	—	A ₁	CI	0	—	—
A ₂	BDI	\mathbb{Z}	A ₂	B_z	A ₂	BDI	\mathbb{Z}	A ₂	B_z
B ₁	BDI	\mathbb{Z}	B ₁	B_y					
B ₂	BDI	\mathbb{Z}	B ₂	B_x					
$p31m, p3m1 (C_{3v}), \bar{E}, \text{spin } 3/2$					$p4m (C_{4v}), \bar{E}_1 \text{ or } \bar{E}_2, \text{spin } 1/2 \text{ or } 3/2$				
IR of Δ	EAZ	1dim.	IR of $\rho_-^{(12)}$	Magetic multipole g_-	IR of Δ	EAZ	1dim.	IR of $\rho_-^{(12)}$	Magetic multipole g_-
A ₁	AIII	\mathbb{Z}	A ₁	$B_x^3 - 3B_xB_y^2$	A ₁	CI	0	—	—
A ₂	D	\mathbb{Z}_2	A ₂	B_z	A ₂	BDI	\mathbb{Z}	A ₂	B_z
					B ₁	AI	0	—	—
					B ₂	AI	0	—	—
$p6m (C_{6v}), \bar{E}_1 \text{ or } \bar{E}_2, \text{spin } 1/2 \text{ or } 5/2$					$p6m (C_{6v}), \bar{E}_3, \text{spin } 3/2$				
IR of Δ	EAZ	1dim.	IR of $\rho_-^{(12)}$	Magetic multipole g_-	IR of Δ	EAZ	1dim.	IR of $\rho_-^{(12)}$	Magetic multipole g_-
A ₁	CI	0	—	—	A ₁	CI	0	—	—
A ₂	BDI	\mathbb{Z}	A ₂	B_z	A ₂	BDI	\mathbb{Z}	A ₂	B_z
B ₁	AI	0	—	—	B ₁	BDI	\mathbb{Z}	B ₁	$B_y^3 - 3B_yB_x^2$
B ₂	AI	0	—	—	B ₂	BDI	\mathbb{Z}	B ₂	$B_x^3 - 3B_xB_y^2$

coincides with that of the gap function. For instance, let us consider $p2 = \{\{e|\mathbf{0}\}, \{2_z|\mathbf{0}\}\}$. In this case, $U_{g,\gamma}$ is

given by

$$U_{\{E|\mathbf{0}\},\gamma} = \begin{pmatrix} 1 & 0 \\ 0 & 1 \end{pmatrix}, \quad U_{\{2_z|\mathbf{0}\},\gamma} = \begin{pmatrix} i & 0 \\ 0 & -i \end{pmatrix}. \quad (67)$$

TABLE III. EAZ symmetry classes, irreps of $\rho_-^{(ab)}$, and magnetic responses for single MKPs for other wallpaper groups including nonsymmorphic ones. Those SGs are explicitly defined by $pg = \{\{e|0\}, \{\sigma_y|\tau_x\}\}$, $cm = \{\{e|0\}, \{\sigma_{(010)}|0\}, \{e|\tau_x\}\}$, $pmg = \{\{e|0\}, \{2_z|0\}, \{\sigma_{(010)}|\tau_x\}, \{\sigma_{(100)}|\tau_x\}\}$, $pgg = \{\{e|0\}, \{2_z|0\}, \{\sigma_{(010)}|\tau_x + \tau_y\}, \{\sigma_{(100)}|\tau_x + \tau_y\}\}$, $cm = \{\{e|0\}, \{2_z|0\}, \{\sigma_{(010)}|0\}, \{\sigma_{(100)}|0\}, \{e|\tau_x + \tau_y\}\}$, $p4g = \{\{e|0\}, \{2_z|0\}, \{4_z|0\}, \{\sigma_{(010)}|\tau_x + \tau_y\}, \{\sigma_{(100)}|\tau_x + \tau_y\}, \{\sigma_{(110)}|\tau_x + \tau_y\}, \{\sigma_{(1\bar{1}0)}|\tau_x + \tau_y\}\}$, where τ_i is a half translation along the i direction, n_z a n -fold rotation around the z axis, $\sigma_{(hkl)}$ a mirror reflection in terms of the (hkl) plane. $\bar{\Gamma}$, \bar{X} , and \bar{M} label $(0,0)$, $(\pi,0)$, and (π,π) points in the surface BZ. We use the notation of irreps in the Bilbao Crystallographic Server [110] when irreps are similar to those in symmorphic groups. On the other hand, irreps of nonsymmorphic groups at the BZ boundary, X_i and X'_i , are given in Table VI.

pg (C_s) $\bar{\Gamma}$ point, $(^1\bar{E}, ^2\bar{E})$, spin 1/2					pg (C_2) \bar{X} point, (X_1, X_1) or (X_2, X_2) , spin 1/2				
IR of Δ	EAZ	1dim.	IR of $\rho_-^{(12)}$	Magnetic multipole g_-	IR of Δ	EAZ	1dim.	IR of $\rho_-^{(12)}$	Magnetic multipole g_-
A	AIII	\mathbb{Z}	A	B_z	A	DIII	\mathbb{Z}_2	A	B_z
B	D	\mathbb{Z}_2	B	B_x, B_y	B	AII	0	—	—
cm (C_s) $\bar{\Gamma}$ point, $(^1\bar{E}, ^2\bar{E})$, spin 1/2					pmg (C_{2v}) $\bar{\Gamma}$ point, \bar{E} , spin 1/2				
IR of Δ	EAZ	1dim.	IR of $\rho_-^{(12)}$	Magnetic multipole g_-	IR of Δ	EAZ	1dim.	IR of $\rho_-^{(12)}$	Magnetic multipole g_-
A	AIII	\mathbb{Z}	A	B_z	A ₁	CI	0	—	—
B	D	\mathbb{Z}_2	B	B_x, B_y	A ₂	BDI	\mathbb{Z}	A ₂	B_z
					B ₁	BDI	\mathbb{Z}	B ₁	B_y
					B ₂	BDI	\mathbb{Z}	B ₂	B_x
pmg (C_{2v}) \bar{X} point, (X'_1, X'_2) or (X'_3, X'_4) , spin 1/2					cm (C_{2v}) $\bar{\Gamma}$ point, \bar{E} , spin 1/2				
IR of Δ	EAZ	1dim.	IR of $\rho_-^{(12)}$	Magnetic multipole g_-	IR of Δ	EAZ	1dim.	IR of $\rho_-^{(12)}$	Magnetic multipole g_-
A ₁	AIII	\mathbb{Z}	A ₁	$B_x B_y B_z$	A ₁	CI	0	—	—
A ₂	A	0	—	—	A ₂	BDI	\mathbb{Z}	A ₂	B_z
B ₁	D	\mathbb{Z}_2	B ₁	B_y	B ₁	BDI	\mathbb{Z}	B ₁	B_y
B ₂	A	0	—	—	B ₂	BDI	\mathbb{Z}	B ₂	B_x
pgg (C_{2v}) $\bar{\Gamma}$ point, \bar{E} , spin 1/2					pgg (C_{2v}) \bar{X} point, (X'_1, X'_2) or (X'_3, X'_4) , spin 1/2				
IR of Δ	EAZ	1dim.	IR of $\rho_-^{(12)}$	Magnetic multipole g_-	IR of Δ	EAZ	1dim.	IR of $\rho_-^{(12)}$	Magnetic multipole g_-
A ₁	CI	0	—	—	A ₁	AIII	\mathbb{Z}	A ₁	$B_x B_y B_z$
A ₂	BDI	\mathbb{Z}	A ₂	B_z	A ₂	A	0	—	—
B ₁	BDI	\mathbb{Z}	B ₁	B_y	B ₁	D	\mathbb{Z}_2	B ₁	B_y
B ₂	BDI	\mathbb{Z}	B ₂	B_x	B ₂	A	0	—	—
$p4g$ (C_{4v}) $\bar{\Gamma}$ point, \bar{E}_1 or \bar{E}_2 , spin 1/2 or 3/2									
IR of Δ	EAZ	1dim.	IR of $\rho_-^{(12)}$	Magnetic multipole g_-					
A ₁	CI	0	—	—					
A ₂	BDI	\mathbb{Z}	A ₂	B_z					
B ₁	AI	0	—	—					
B ₂	AI	0	—	—					

Substituting Eq. (67) into Eq. (40), we find

$$\chi_{\{e|0\}}^\Omega = 1, \quad \chi_{\{2_z|0\}}^\Omega = \eta_{2_z}, \quad (68)$$

which reproduces Eq.(52). We summarize the obtained irreps of $\rho_-^{(ab)}$ in Tables II and III. We note that the minimal set is double MKPs when MFs are positioned at the \bar{M} point of pgg or $p4g$. As explained in Sec.III C, the double MKPs originate from a crystalline symmetry-enforced fourfold degeneracy. In the following, we focus on magnetic responses in the single MKP cases. The elec-

tromagnetic responses for double MKPs will be discussed in Sec. VI.

For a single MKP, a nonzero $\hat{\mathcal{O}}_{\text{MF}}$ is always odd under TRS (see arguments in Sec.III D). Hence, the magnetic coupling is given by

$$\hat{H}_{\text{m}} = \int d\mathbf{x} g_{-}(\mathbf{B}) \hat{\mathcal{O}}_{\text{MF}-}(\mathbf{x}), \quad (69)$$

where

$$g_-(\mathbf{B}) = \sum_i c_{1,i} B_i + \sum_{ijk} c_{3,ijk} B_i B_j B_k + \dots \quad (70)$$

Here $c_{1,i}$ and $c_{3,ijk}$ are material dependent parameters subject to constraints from crystalline symmetry. The symmetry-adopted forms of $g_-(\mathbf{B})$ are listed in Table VII, where the first, third, fifth, and seventh order of magnetic fields correspond to a magnetic dipole, octupole, 32-pole, and 128-pole, respectively. As argued in Sec. III E, $g_-(\mathbf{B})$ should be the same irrep as $\rho_-^{(12)}$.

For instance, let us consider $p2$. When the irrep of the gap function is A, the irrep of $\rho_-^{(12)}$ is also A. Thus an allowed \mathcal{O} satisfies

$$\mathcal{U}_{\{2_z|0\}} \mathcal{O}_{p2-}^A \mathcal{U}_{\{2_z|0\}}^\dagger = \mathcal{O}_{p2-}^A, \quad \mathcal{T} \mathcal{O}_{p2-}^A \mathcal{T}^{-1} = -\mathcal{O}_{p2-}^A, \quad (71)$$

and $g_-(\mathbf{B})$ is given by

$$g_{p2-}^A(\mathbf{B}) = c_1 B_z, \quad (72)$$

since a magnetic field is transformed as $(B_x, B_y, B_z) \rightarrow (-B_x, -B_y, B_z)$ under $\{2_z|0\}$. Hence \hat{H}_m reads

$$\hat{H}_m = c_1 \int d\mathbf{x} B_z \hat{\mathcal{O}}_{\text{MF } p2-}^A, \quad (73)$$

where $\hat{\mathcal{O}}_{\text{MF } p2-}^A$ is defined by Eq.(28) with $\mathcal{O} = \mathcal{O}_{p2-}^A$. This term provides the magnetic dipole response of the MKP along the rotation axis. Such a magnetic response has been known for superfluid $^3\text{He-B}$ phase [47, 69, 70, 72], and the E_{1u} state of UPt_3 [73]. On the other hand, for the B gap function, \mathcal{O} for the MKP satisfies

$$\mathcal{U}_{\{2_z|0\}} \mathcal{O}_{p2-}^B \mathcal{U}_{\{2_z|0\}}^\dagger = -\mathcal{O}_{p2-}^B. \quad (74)$$

Thus, the lowest order of $g_-(\mathbf{B})$ is given by

$$g_{p2-}^B(\mathbf{B}) = c_{1,1} B_x + c_{1,2} B_y, \quad (75)$$

resulting in the magnetic dipole response parallel to the surface. The direction of the dipole response depends on the material dependent parameters $c_{1,i}$ ($i = 1, 2$).

In this manner, we can determine possible magnetic responses of a single MKP protected by all paper groups, which are summarized in Tables II and III. We find that a single MKP shows magnetic dipole responses in most cases: In addition to the $^3\text{He-B}$ phase and the E_{1u} state of UPt_3 mentioned in the above, the A_{1u} state of the superconducting doped topological insulator [52] also shows the magnetic dipole response. For the (111) surface of the doped topological insulator, which is normal to the z -direction, there exists a single MKP at the $\bar{\Gamma}$ point of the surface BZ. Because the (111) surface hosts C_{3v} symmetry, and the A_{1u} gap function is the A_2 irrep for C_{3v} , from Table II, we find that the surface MKP has the magnetic dipole parallel to the z -direction.

Interestingly, our result shows that magnetic octupole responses are also possible. The rest of this section focuses on the magnetic octupole responses, which are realized in spin 3/2 TSCs and nonsymmorphic TSCs.

B. Magnetic octupole response of spin 3/2 MFs

The spin of MKPs is effectively given by 1/2, 3/2, and 5/2, each of which forms different irreps. There exist magnetic structures allowed only for the spin 3/2 MFs when the wallpaper group including the threefold rotation symmetry.

For example, let us consider the case with $p3m1 = \{\{e|0\}, \{3_z|0\}, \{\sigma_{(100)}|0\}\}$ and the A_1 gap function. Here $\{3_z|0\}$ is a threefold rotation about the z axis and $\{\sigma_{(100)}|0\}$ is a mirror-reflection with respect to the (100) plane. From Table II, the irrep of $\rho_-^{(12)}$ is A_1 . Thus, \mathcal{O}_- coupled to the spin-3/2 MKP satisfies

$$\mathcal{U}_{\{3_z|0\}} \mathcal{O}_{p3m1-}^{A_1} \mathcal{U}_{\{3_z|0\}}^\dagger = \mathcal{O}_{p3m1-}^{A_1}, \quad (76a)$$

$$\mathcal{U}_{\{\sigma_{(100)}|0\}} \mathcal{O}_{p3m1-}^{A_1} \mathcal{U}_{\{\sigma_{(100)}|0\}}^\dagger = \mathcal{O}_{p3m1-}^{A_1}. \quad (76b)$$

The magnetic field changes as $\{3_z|0\} : (B_+, B_-, B_z) \rightarrow (e^{i\frac{2\pi}{3}} B_+, e^{-i\frac{2\pi}{3}} B_-, B_z)$ and $\{\sigma_{(100)}|0\} : (B_x, B_y, B_z) \rightarrow (B_x, -B_y, -B_z)$ under the operations of $p3m1$, where $B_+ \equiv B_x + iB_y$, $B_- \equiv B_x - iB_y$. Since the irrep of $g_-(\mathbf{B})$ has to be A_1 , it is of the form:

$$g_{p3m1-}^{A_1}(\mathbf{B}) = c_3 (B_x^3 - 3B_x B_y^2), \quad (77)$$

which gives the magnetic octupole response as a leading contribution. It should be noted here that the three-fold rotation symmetry forbids the first order term of B_i . In a similar manner, the magnetic octupole response appears for $p6m$ when the spin of MKPs is 3/2 and the irrep of the gap functions is the B_1 or B_2 gap function. The $g_-(\mathbf{B})$'s in the lowest order are

$$g_{p6m-}^{B_1}(\mathbf{B}) = c_3 (B_y^3 - 3B_y B_x^2), \quad (78)$$

$$g_{p6m-}^{B_2}(\mathbf{B}) = c_3 (B_x^3 - 3B_x B_y^2). \quad (79)$$

In the previous study [76], we pointed out that the magnetic octupole response is realized in the half-Hausler superconductors [88–94] with the A_1 gap function of T_d in the (111) surface. On the surface, the A_1 irrep of T_d is compatible with the A_1 irrep of C_{3v} ($p31m$ or $p3m1$ in the wallpaper groups). The similar compatible relation is met in the A_{2u} irrep of O_h . Hence the antiperovskite Dirac metals [63, 64] with the A_{2u} gap function of O_h are also a possible candidate for this response.

In $p6$ symmetric TSCs with the B gap function, we have a slightly different magnetic octupole response. As is the case with $p3m1$, the spin-3/2 state is necessary, but the MKP is stabilized by a \mathbb{Z}_2 invariant. \mathcal{O}_- for the MKP only respects

$$\mathcal{U}_{\{6_z|0\}} \mathcal{O}_{p6-}^B \mathcal{U}_{\{6_z|0\}}^\dagger = -\mathcal{O}_{p6-}^B. \quad (80)$$

Therefore, the magnetic octupole response is described by

$$g_{p6-}^B(\mathbf{B}) = c_{3,1} (B_x^3 - 3B_x B_y^2) + c_{3,2} (B_y^3 - 3B_y B_x^2). \quad (81)$$

In the polar coordinate $(B_x, B_y) = B(\cos \phi, \sin \phi)$, it is rewritten as

$$g_{p6-}^B(\mathbf{B}) = c_{3,1} B^3 \cos(3\phi + \theta_\rho), \quad (82)$$

where $\tan \theta_\rho = c_{3,2}/c_{3,1}$. Since the magnetic response preserves only the sixfold rotation symmetry, it can be tilted by the material dependent angle θ_ρ . Interestingly, this type of the magnetic octupole response is realized in fully-gapped TSCs as we will show in Sec. V A.

C. Magnetic octupole response by nonsymmorphic symmetry

We show another mechanism realizing the magnetic octupole response. The key ingredient is the glide symmetry, which appears in pg , pmg , pgg , and $p4g$.

For example, we consider the case with $pmg = \{\{e|\mathbf{0}\}, \{2_z|\mathbf{0}\}, \{\sigma_{(010)}|\tau_x\}\}$ and the A_1 gap function. The irrep of \mathcal{O} for the MKP at $\bar{\Gamma}$ point is different from that at \bar{X} point since the factor system for glide $\{\sigma_{(010)}|\tau_x\}$ has an additional phase at the \bar{X} point. From Table III, we have a \mathbb{Z} invariant at the \bar{X} point while there is no topological invariant at the $\bar{\Gamma}$ point. When the irrep of \mathcal{O}_- is A_1 , it satisfies

$$\mathcal{U}_{\{2_z|\mathbf{0}\}} \mathcal{O}_{pmg}^{A_1} \mathcal{U}_{\{2_z|\mathbf{0}\}}^\dagger = \mathcal{O}_{pmg-}^{A_1}, \quad (83a)$$

$$\mathcal{U}_{\{\sigma_y|\tau_x\}} \mathcal{O}_{pmg-}^{A_1} \mathcal{U}_{\{\sigma_y|\tau_x\}}^\dagger = \mathcal{O}_{pmg-}^{A_1}. \quad (83b)$$

On the other hand, the magnetic field changes as

$$\{2_z|\mathbf{0}\} : (B_x, B_y, B_z) \rightarrow (-B_x, -B_y, B_z), \quad (84a)$$

$$\{\sigma_y|\tau_x\} : (B_x, B_y, B_z) \rightarrow (-B_x, B_y, -B_z). \quad (84b)$$

As $g_-(\mathbf{B})$ for the magnetic coupling should be the same irrep as \mathcal{O}_- , it is given by

$$g_{pmg-}^{A_1}(\mathbf{B}) = c_3 B_x B_y B_z, \quad (85)$$

which represents the magnetic octupole response.

V. MAJORANA OCTUPOLE RESPONSES IN TIGHT-BINDING MODELS

In this section, using concrete models, we demonstrate magnetic octupole responses in $p6$ and pmg , which have been overlooked so far.

A. Model with $p6$ symmetry

We consider a tight-binding model with space group $P622$ (SG# 177), which is built on the triangular lattice with p_x , p_y , and p_z orbitals on each site. The normal Hamiltonian is given by

$$h_{p6}(\mathbf{k}) = h_0(\mathbf{k}) + h_{\text{soc}}(\mathbf{k}), \quad (86)$$

with

$$h_0(\mathbf{k}) = m_0 + m_1 \lambda_8 + t_z \cos k_z + t_{xy} \left\{ \cos k_x + 2 \cos \left(\frac{k_x}{2} \right) \cos \left(\frac{\sqrt{3}k_y}{2} \right) \right\}, \quad (87a)$$

$$h_{\text{soc}}(\mathbf{k}) = \alpha \cos k_z (\lambda_5 s_y - \lambda_7 s_x) + \beta \sin k_z (\lambda_4 s_x + \lambda_6 s_y) + \gamma (\sin k_x s_x + \sin k_y s_y), \quad (87b)$$

where λ_i ($i = 1 - 8$) are the Gell-Mann matrices acting on the (p_x, p_y, p_z) orbitals, and s_i are the Pauli matrices in the spin space. m_0 and m_1 are on-site potentials, t_z and t_{xy} are hopping terms, and α , β , and γ represent spin-orbital interactions. The normal Hamiltonian hosts TRS and the $P622$ symmetry below,

$$U_{\{6_z|\mathbf{0}\}} h_{p6}(\mathbf{k}) U_{\{6_z|\mathbf{0}\}}^\dagger = h_{p6}(6_z \mathbf{k}), \quad (88a)$$

$$U_{\{2_y|\mathbf{0}\}} h_{p6}(\mathbf{k}) U_{\{2_y|\mathbf{0}\}}^\dagger = h_{p6}(2_y \mathbf{k}), \quad (88b)$$

$$U_{\{2_x|\mathbf{0}\}} h_{p6}(\mathbf{k}) U_{\{2_x|\mathbf{0}\}}^\dagger = h_{p6}(2_x \mathbf{k}), \quad (88c)$$

with

$$U_{\{6_z|\mathbf{0}\}} = R_z \left(\frac{2\pi}{6} \right) \exp \left(-i s_z \frac{\pi}{6} \right), \quad (89a)$$

$$U_{\{2_y|\mathbf{0}\}} = R_y(\pi)(-i s_y), \quad (89b)$$

$$U_{\{2_x|\mathbf{0}\}} = R_x(\pi)(-i s_x), \quad (89c)$$

where $R_i(\theta)$ is a 3×3 rotation matrix in the basis (p_x, p_y, p_z) and represents the θ rotation about the i axis. The band structure of Eq. (86) is shown in Fig. 1 (a). When $\beta = \gamma = 0$, the normal Hamiltonian recovers the spatial inversion, giving three doubly degenerate bands: one band is effectively described by spin 3/2 electrons, whereas the other bands are described by spin 1/2 electrons. When $\beta \neq 0$ and $\gamma \neq 0$, the doubly degenerate bands are split due to the breaking of spatial inversion. In the following, we choose the chemical potential such that the spin 3/2 band forms the Fermi surface around the Γ point. For the superconducting state, we consider the B_1 and B_2 gap functions:

$$\Delta_{B_1}(\mathbf{k}) = \Delta_0 (\eta_1 \sin k_z (\lambda_1 s_x + \lambda_3 s_y) + \eta_2 f_x(\mathbf{k}) \lambda_2) (i s_y), \quad (90a)$$

$$\Delta_{B_2}(\mathbf{k}) = \Delta_0 (\eta'_1 \sin k_z (\lambda_1 s_y - \lambda_3 s_x) + \eta'_2 f_y(\mathbf{k}) \lambda_2) (i s_y), \quad (90b)$$

where $f_x(\mathbf{k}) = \left(\sin k_x - 2 \sin \left(\frac{k_x}{2} \right) \cos \left(\frac{\sqrt{3}k_y}{2} \right) \right)$ and $f_y(\mathbf{k}) = \left(\sin k_y - 2 \sin \left(\frac{k_y}{2} \right) \cos \left(\frac{\sqrt{3}k_x}{2} \right) \right)$, and η_1, η_2, η'_1 , and η'_2 are real parameters. When the gap function is Δ_{B_1} (Δ_{B_2}), there appear point nodes in the k_y axis (the k_x axis), which are protected by $\{2_y|\mathbf{0}\}$ ($\{2_x|\mathbf{0}\}$) rotation symmetry. On the (001) plane, the zero energy flatband states connecting the point nodes appear because a 2d \mathbb{Z}_2 invariant becomes non-trivial between the point nodes.

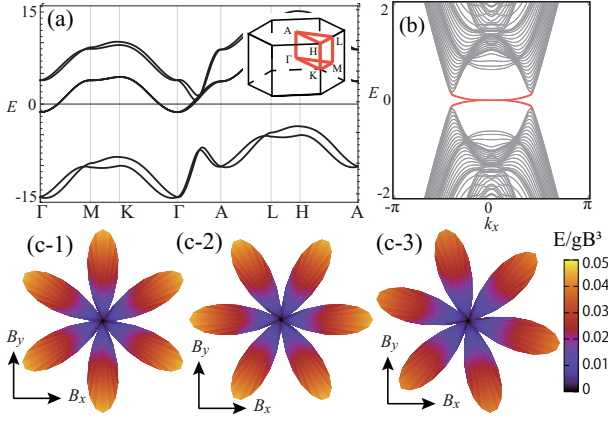


FIG. 1. (a) The band structure of Eq. (86) with parameters $(m_0, m_1, t_{xy}, t_z, \alpha, \beta, \gamma) = (2.2, 5, -1.3, -2.5, 6, 0.5, 1)$. (b) The (001) surface state in the fully-gapped superconducting states. Here, we choose the chemical potential and the amplitude of the gap function as $\mu = 0$ and $\Delta_0 = 1$ and the B_1 and B_2 gap functions coexist such that $\eta_1 = \eta_2 = \eta'_1 = \eta'_2 = 0.5$. (c) Applying the Zeeman magnetic field $h_Z = g\mathbf{B} \cdot \mathbf{s}$, the energy gap of the MKP is illustrated as a function of \mathbf{B} : (c-1) Δ_{B_1} only, (c-2) Δ_{B_2} only, and (c-3) the mixture of Δ_{B_1} and Δ_{B_2} .

We here focus on the MKP at the $\bar{\Gamma}$ point ($k_x = k_y = 0$). Since B_1 and B_2 in $P622$ are compatible with B in $p6$ on the surface. Hence, our theory predicts the magnetic octupole response there. To demonstrate this, we add the Zeeman magnetic field $h_Z = g\mathbf{B} \cdot \mathbf{s}$ in the normal Hamiltonian and numerically calculate the energy gap of the MKP as a function of \mathbf{B} . See Figs. 1 (c-1) and (c-2). The magnetic responses keep sixfold rotation symmetry and behaves like Eq. (77). The magnetic octupole response is unique to the spin 3/2 electrons because a point node appears at $k_x = k_y = 0$ if the chemical potential lies on the spin 1/2 electrons [109].

Furthermore, if the $P622$ symmetry is broken to the $P6$ symmetry, the Δ_{B_1} and Δ_{B_2} gap functions can coexist, and the BdG Hamiltonian realizes a fully-gap TSC. A MKP exists at $k_x = k_y = 0$ (see Fig. 1 (b)), which shows a tilted magnetic octupole response as shown in Fig. 1 (c-3). The magnetic response respects the sixfold rotation symmetry, but zeros of the energy gap appear according to Eq. (81) with nonzero θ_ρ .

B. Model with pmg symmetry

So far, we consider surface MFs in 3d topological superconductors, but our theory also works for MFs in lower dimensional systems. Here we consider a 2d model with pmg symmetry, which host a single MKP showing a magnetic octupole response.

Let us consider the 2d square lattice with $Pma2$ (SG# 28) [77, 112]. In the unit cell, we have two atoms located at $(0, 0, -z)$ and $(1/2, 0, z)$. Provided that only the s

orbital exists on each site, the tight-binding model is

$$h_{pmg}(\mathbf{k}) = h_0(\mathbf{k}) + h_{soc}(\mathbf{k}), \quad (91)$$

with

$$h_0(\mathbf{k}) = m_0 + t_1 \cos k_x + t_2 \cos k_y + t_3 \cos \left(\frac{k_x}{2} \right) \sigma_x(k_x), \quad (92a)$$

$$h_{soc}(\mathbf{k}) = (\alpha \sin k_y s_x + \beta \sin k_x s_y) \sigma_z + \gamma \left(\sin \left(\frac{k_x}{2} \right) \sigma_x(k_x) s_z + \cos \left(\frac{k_x}{2} \right) \sigma_y(k_x) s_x \right), \quad (92b)$$

where s_i and σ_i ($i = x, y, z$) are Pauli matrices describing the spin and the sublattice degrees of freedom, and $\sigma_x(k_x)$ and $\sigma_y(k_x)$ are modified Pauli matrices:

$$\sigma_x(k_x) \equiv \begin{pmatrix} 0 & e^{ik_x/2} \\ e^{-ik_x/2} & 0 \end{pmatrix}, \quad (93a)$$

$$\sigma_y(k_x) \equiv \begin{pmatrix} 0 & -ie^{ik_x/2} \\ ie^{-ik_x/2} & 0 \end{pmatrix}. \quad (93b)$$

m_0 is an on-site potential, t_1 and t_2 are in-plane hopping terms, t_3 represents a hopping between the different atoms, α and β are in-plane spin-orbit interactions, and γ is spin-orbit interactions between the different atoms. Equation (91) respects TRS and the following crystal symmetries:

$$U_{\{2_y|0\}} h_{pmg}(\mathbf{k}) U_{\{2_y|0\}}^\dagger = h_{pmg}(2_y \mathbf{k}), \quad (94a)$$

$$U_{\{\sigma_{(001)}|\tau_x\}} h_{pmg}(\mathbf{k}) U_{\{\sigma_{(001)}|\tau_x\}}^\dagger = h_{pmg}(\sigma_{(001)} \mathbf{k}), \quad (94b)$$

$$U_{\{\sigma_{(100)}|\tau_x\}} h_{pmg}(\mathbf{k}) U_{\{\sigma_{(100)}|\tau_x\}}^\dagger = h_{pmg}(\sigma_{(100)} \mathbf{k}), \quad (94c)$$

with

$$U_{\{2_y|0\}} = -i\sigma_x s_y, \quad (95a)$$

$$U_{\{\sigma_{(001)}|\tau_x\}} = \begin{pmatrix} 0 & e^{ik_x} \\ 1 & 0 \end{pmatrix} (is_z), \quad (95b)$$

$$U_{\{\sigma_{(100)}|\tau_x\}} = \begin{pmatrix} e^{ik_x} & 0 \\ 0 & 1 \end{pmatrix} (is_x). \quad (95c)$$

We show the band structure of Eq. (91) in Fig. 2 (a), where the glide symmetry-protected band crossing appears on the lines $\Gamma - X$ and $Y - M$. For the superconducting state, we consider the A_1 gap function:

$$\Delta_{A_1} = \Delta_0 \left(\eta_1 \sin k_y \sigma_z s_x + \eta_2 \sin \left(\frac{k_x}{2} \right) \sigma_x(k_x) s_z \right) (is_y). \quad (96)$$

Numerically diagonalizing the BdG Hamiltonian with the open boundary condition in the y direction, we obtain a single MKP at $k_x = \pi$ as shown in Fig. 2 (b). Whereas

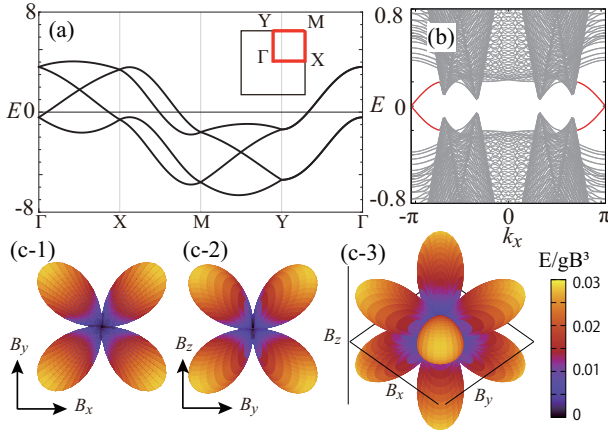


FIG. 2. (a) The band structure of Eq. (91) with parameters $(m_0, t_1, t_2, t_3, \alpha, \beta, \gamma) = (-1, 0.1, 2.5, 0.25, -1, 0.3, 2)$. (b) The (01) surface state in the superconducting state with $\mu = 1$, $\Delta_0 = 1$, $\eta_1 = 0.5$, and $\eta_2 = 0.1$. (c) The energy gap of the MKP as a function of \mathbf{B} under the Zeeman magnetic field $h_Z = g\mathbf{B} \cdot \mathbf{s}$: The view from (c-1) [001], (c-2) [100], and (c-3) [111] directions.

the open boundary condition breaks the two-fold rotation symmetry in Eq. (94a), it keeps pmg symmetry generated by Eqs. (94b) and (94c). Then, regarding the $k_x = \pi$ point as the \bar{X} point (and exchanging the y and the z directions in Table III), we can use the result in Table III, which predicts the magnetic octupole response in the form of Eq. (85). In Fig. 2 (c), we show the magnetic response obtained by adding the Zeeman magnetic term $h_Z = g\mathbf{B} \cdot \mathbf{s}$ in the normal Hamiltonian. This result is consistent with Eq. (85).

VI. MKPS AT \bar{M} POINT IN pgg AND $p4g$

So far, we have considered magnetic responses of a single MKP, which is valid except for the wallpaper groups pgg and $p4g$. For the pgg and $p4g$ symmetries at the \bar{M} point, TRS and crystalline symmetry ensure a four-fold degenerate band crossing on surfaces, realizing two MKPs. In the following, we discuss electromagnetic structures arising from those two MKPs.

When there are two MKPs, both $\rho_+^{(ab)}$ and $\rho_-^{(ab)}$ are nonzero, and thus both electric and magnetic couplings are possible. Using Eq. (55), we determine the electric and magnetic couplings.

A. short representation

In the present cases, Eq. (52) is not available. To evaluate Eq. (55), we explicitly construct the representation

$U_{g,\gamma}$, T_γ , C_γ and Γ_γ defined below,

$$\begin{aligned} \mathcal{U}_g^{\mathbf{k}} |u_0^{(a)}\rangle &= \sum_b |u_0^{(b)}\rangle [U_{g,\gamma}]_{ba}, \\ \mathcal{T} |u_0^{(a)}\rangle &= \sum_b |u_0^{(b)}\rangle [T_\gamma]_{ba}, \\ \mathcal{C} |u_0^{(a)}\rangle &= \sum_b |u_0^{(b)}\rangle [C_\gamma]_{ba}, \\ \Gamma |u_0^{(a)}\rangle &= \sum_b |u_0^{(b)}\rangle [\Gamma_\gamma]_{ba}. \end{aligned} \quad (97)$$

Here $\Gamma_\gamma = -iT_\gamma C_\gamma^*$ since $\Gamma = -i\mathcal{T}\mathcal{C}$. Whereas $U_{g,\gamma}$, T_γ , C_γ , and Γ_γ obey the same multiplication law as $\mathcal{U}_g^{\mathbf{k}}$, \mathcal{T} , \mathcal{C} and Γ , the dimension of the representation becomes half, as explained shortly.

Let us start with a zero mode $|u_0^{(a)}\rangle$ belonging to an irrep α of $G_0^{\mathbf{k}}$. Using the Wigner test W_α^T , we can obtain a co-representation of $G_0^{\mathbf{k}} + TG_0^{\mathbf{k}}$ from the irrep α , in the standard manner. However, to obtain a representation of $G^{\mathbf{k}} = G_0^{\mathbf{k}} + TG_0^{\mathbf{k}} + CG_0^{\mathbf{k}} + \Gamma G_0^{\mathbf{k}}$, we also need to take into account either PHS or CS. If either PHS or CS is taken into account, another one is automatically included, because $\Gamma = -i\mathcal{T}\mathcal{C}$.

To include these antisymmetries, we refer to the EAZ class of α . The zero mode $|u_0^{(a)}\rangle$ can exist in the irrep α when the EAZ class has a non-trivial topological invariant \mathbb{Z} or \mathbb{Z}_2 . If the topological invariant is \mathbb{Z} , the irrep α keeps CS, and the zero mode can be an eigenstate of Γ , say $\Gamma |u_0^{(a)}\rangle = |u_0^{(a)}\rangle$, in a proper basis. On the other hand, if the topological invariant is \mathbb{Z}_2 , the irrep α keeps PHS, and the zero mode can satisfy $\mathcal{C} |u_0^{(a)}\rangle = |u_0^{(a)}\rangle$ in a proper basis. In this manner, the action of CS or PHS to the zero mode is determined by referring to the EAZ class. Using the relation $\{\Gamma, \mathcal{T}\} = 0$ and $[\mathcal{C}, \mathcal{T}] = 0$, we can also generalize this argument to the co-representation obtained from α , which provides a representation of $G^{\mathbf{k}}$.

For instance, let us consider MKPs at the \bar{M} point of pgg . We also assume that the irrep of the gap function is A_1 . As a fermion, MFs belong to a double-valued representation, which is uniquely given by the M irrep in Table VI. The M irrep is two-dimensional and obeys

$$\begin{aligned} U_{\{2_z|\mathbf{0}\},\gamma}^2 &= -1, \\ U_{\{\sigma_{(010)}|\boldsymbol{\tau}_x+\boldsymbol{\tau}_y\},\gamma}^2 &= 1, \\ U_{\{\sigma_{(100)}|\boldsymbol{\tau}_x+\boldsymbol{\tau}_y\},\gamma}^2 &= 1, \end{aligned} \quad (98)$$

together with the other standard commutation relations between the generators. When the gap function belongs to the A_1 irrep, these generators also commute with PHS \mathcal{C} . As shown in Table III, the Wigner test indicates that the EAZ class is DIII, of which topological invariant is \mathbb{Z}_2 . Thus, we can take the basis satisfying the condition $\mathcal{C} |u_0^{(a)}\rangle = |u_0^{(a)}\rangle$. Because $U_{\{\sigma_{(100)}|\boldsymbol{\tau}_x+\boldsymbol{\tau}_y\},\gamma}$ commutes with \mathcal{C} and has real eigenvalues ± 1 , the eigenbasis of $U_{\{\sigma_{(010)}|\boldsymbol{\tau}_x+\boldsymbol{\tau}_y\},\gamma}$ satisfies the above condition. Moreover, to take into account TRS, we add another M irrep of MFs

TABLE IV. Short representation of double MKPs at the \bar{M} point for pgg and $p4g$. Matrix representations of other elements in $p4g$ are given by the product of them, e.g., $U_{\{\sigma_{(110)}|\tau_x+\tau_y\},\gamma} = U_{\{\sigma_{(100)}|\tau_x+\tau_y\},\gamma}U_{\{4_z|\mathbf{0}\},\gamma}$.

$pgg \bar{M}$ point							
IR of Δ	$U_{\{e \mathbf{0}\},\gamma}$	$U_{\{2_z \mathbf{0}\},\gamma}$	$U_{\{\sigma_{(010)} \tau_x+\tau_y\},\gamma}$	$U_{\{\sigma_{(100)} \tau_x+\tau_y\},\gamma}$	T_γ	C_γ	Γ_γ
A_1	$\sigma_0 s_0$	$i\sigma_y s_0$	$\sigma_x s_0$	$\sigma_z s_0$	$i\sigma_0 s_y$	$\sigma_0 s_0$	$\sigma_0 s_y$
A_2	$\sigma_0 s_0$	$i\sigma_z s_0$	$\sigma_y s_0$	$\sigma_x s_0$	$i\sigma_x s_y$	$\sigma_y s_y$	$\sigma_z s_0$
B_1	$\sigma_0 s_0$	$i\sigma_x s_0$	$\sigma_z s_0$	$\sigma_y s_0$	$i\sigma_z s_y$	$\sigma_0 s_0$	$\sigma_z s_y$
B_2	$\sigma_0 s_0$	$i\sigma_x s_0$	$\sigma_y s_0$	$\sigma_z s_0$	$i\sigma_z s_y$	$\sigma_0 s_0$	$\sigma_z s_y$

$p4g \bar{M}$ point							
IR of Δ	$U_{\{e \mathbf{0}\},\gamma}$	$U_{\{4_z \mathbf{0}\},\gamma}$	$U_{\{2_z \mathbf{0}\},\gamma}$	$U_{\{\sigma_{(100)} \tau_x+\tau_y\},\gamma}$	T_γ	C_γ	Γ_γ
A_1	$\sigma_0 s_0$	$e^{i\pi(2\sigma_0 s_z + \sigma_z s_z)/4}$	$-i\sigma_z s_z$	$\sigma_x s_0$	$i\sigma_0 s_y$	$\sigma_0 s_x$	$\sigma_0 s_z$
A_2	$\sigma_0 s_0$	$e^{i\pi(2\sigma_0 s_z + \sigma_z s_z)/4}$	$-i\sigma_z s_z$	$\sigma_x s_0$	$i\sigma_0 s_y$	$\sigma_z s_x$	$\sigma_z s_z$
B_1	$\sigma_0 s_0$	$e^{i\pi(2\sigma_0 s_z + \sigma_z s_z)/4}$	$-i\sigma_z s_z$	$\sigma_x s_0$	$i\sigma_0 s_y$	$\sigma_x s_0$	$\sigma_x s_y$

according to the Wigner test of TRS. Consequently, we obtain

$$\begin{aligned}
 U_{\{2_z|\mathbf{0}\},\gamma} &= i\sigma_y s_0, \quad U_{\{\sigma_{(010)}|\tau_x+\tau_y\},\gamma} = \sigma_x s_0, \\
 U_{\{\sigma_{(100)}|\tau_x+\tau_y\},\gamma} &= \sigma_z s_0, \quad C_\gamma = \sigma_0 s_0, \quad T_\gamma = i\sigma_0 s_y.
 \end{aligned} \tag{99}$$

It should be noted here that PHS and CS do not increase the dimension of the representation. This is sharp contrast to the representation for ordinary electron systems. For ordinary systems, PHS and CS transform an electron to an hole, and thus to realize these symmetries, we need to consider the corresponding holes at the same time, which doubles the degrees of freedom. In contrast, in the case of MFs, we do not need to double the degrees of freedom since MFs are their own anti-particles. These antisymmetries map MFs to themselves. As a result, MFs provide a representation shorter than that for ordinary electrons. The short representation is a central property of MFs, which is a group theoretical manifestation of the self-conjugate property of MFs. In a different context, a similar short representation has been known for the BPS states in supersymmetric theories [113]. In Table IV, we summarize the short representation of MKPs at the \bar{M} point for pgg and $p4g$.

B. electric and magnetic responses

Using Eq.(55), we can determine possible electric and magnetic couplings of the double MKPs at the \bar{M} point for pgg and $p4g$. For instance, let us consider pgg and the A_1 gap function. From the short representation in

Table IV, $\chi_g^{\Omega^\pm}$ reads

$$\begin{aligned}
 \chi_{\{e|\mathbf{0}\}}^{\Omega^+} &= 2, \quad \chi_{\{e|\mathbf{0}\}}^{\Omega^-} = 4, \\
 \chi_{\{2_z|\mathbf{0}\}}^{\Omega^+} &= 2, \quad \chi_{\{2_z|\mathbf{0}\}}^{\Omega^-} = 0, \\
 \chi_{\{\sigma_{(010)}|\tau_x+\tau_y\}}^{\Omega^+} &= -2, \quad \chi_{\{\sigma_{(010)}|\tau_x+\tau_y\}}^{\Omega^-} = 0, \\
 \chi_{\{\sigma_{(100)}|\tau_x+\tau_y\}}^{\Omega^+} &= -2, \quad \chi_{\{\sigma_{(100)}|\tau_x+\tau_y\}}^{\Omega^-} = 0.
 \end{aligned} \tag{100}$$

Then, using the standard group theoretical method, we perform the irreducible decomposition of $\rho_\pm^{(ab)}$ in terms of the single-valued irreps of C_{2v} ,

$$\rho_+^{(ab)} = 2A_2, \quad \rho_-^{(ab)} = A_1 + A_2 + B_1 + B_2. \tag{101}$$

Because $\rho_+^{(ab)} \neq 0$, in contrast to a single MKP, the double MKPs may host an electric response. We find that the electric response is quadrupole. As explained in Sec.III E, $f(\mathbf{E})$ in Eq.(66) shares the same irrep with $\rho_+^{(ab)}$. Thus, referring to irreps of $f(\mathbf{E})$ in Table VIII, we find

$$f_{pgg}^{A_2}(\mathbf{E}) = c_2 E_x E_y, \tag{102}$$

with a constant c_2 , which is quadrupole. We can also evaluate the magnetic response of the double MKPs. Since $g_+(\mathbf{B})$ and $g_-(\mathbf{B})$ in Eq.(63) are possible, their leading terms are given by

$$\begin{aligned}
 g_{pgg+}^{A_2}(\mathbf{B}) &= c_{2+} B_x B_y, \\
 g_{pgg-}^{A_1}(\mathbf{B}) &= c_{3-} B_x B_y B_z, \\
 g_{pgg-}^{A_2}(\mathbf{B}) &= c_{1,1-} B_z, \\
 g_{pgg-}^{B_1}(\mathbf{B}) &= c_{1,2-} B_y, \\
 g_{pgg-}^{B_2}(\mathbf{B}) &= c_{1,3-} B_x,
 \end{aligned} \tag{103}$$

where c_{2+} , c_{3-} , and $c_{1,i-}$ are material dependent parameters. This result implies that the leading magnetic response of the double MKPs is a mixture of dipole and quadrupole.

TABLE V. EAZ symmetry classes, irreps of $\rho_{\pm}^{(ab)}$, and electric and magnetic responses of the double MKPs at the \bar{M} point for pgg and $p4g$.

$pgg (C_{2v}) \bar{M} \text{ point, } (M, M)$					
IR of Δ	IR of $\rho_{+}^{(ab)}$	IR of $\rho_{-}^{(ab)}$	Electric multipole f	Electric multipole g_{+}	Magnetic multipole g_{-}
A_1	$2A_2$	$A_1 + A_2 + B_1 + B_2$	$E_x E_y$	$B_x B_y$	$B_x, B_y, B_z, B_x B_y B_z$
A_2	$B_1 + B_2$	$3A_1 + A_2$	E_x, E_y	$B_x B_z, B_y B_z$	$B_z, B_x B_y B_z$
B_1	$A_2 + B_2$	$A_1 + B_1 + 2B_2$	$E_y, E_x E_y$	$B_x B_y, B_y B_z$	$B_x, B_y, B_x B_y B_z$
B_2	$A_2 + B_1$	$A_1 + 2B_1 + B_2$	$E_x, E_x E_y$	$B_x B_y, B_x B_z$	$B_x, B_y, B_x B_y B_z$
$p4g (C_{4v}) \bar{M} \text{ point, } (M_1, M_2)$					
IR of Δ	IR of $\rho_{+}^{(ab)}$	IR of $\rho_{-}^{(ab)}$	Electric multipole f	Electric multipole g_{+}	Magnetic multipole g_{-}
A_1	$2B_2$	$A_1 + A_2 + E$	$E_x E_y$	$B_x B_y$	$B_z, \{B_x, B_y\}, B_x B_y B_z (B_x^2 - B_y^2)$
A_2	E	$A_1 + A_2 + 2B_1$	$\{E_x, E_y\}$	$\{B_x B_z, B_y B_z\}$	$B_z, B_x B_y B_z, B_x B_y B_z (B_x^2 - B_y^2)$
B_1	$A_2 + B_2$	$A_2 + B_1 + E$	$E_x E_y, E_x E_y (E_x^2 - E_y^2)$	$B_x B_y, B_x B_y (B_x^2 - B_y^2)$	$B_z, \{B_x, B_y\}, B_x B_y B_z$
B_2	—	—	—	—	—

In a similar manner, we calculate $\chi_g^{\Omega\pm}$ for all possible double MKPs at the \bar{M} point in pgg and $p4g$, and evaluate possible electric and magnetic responses. The obtained electric and magnetic responses are summarized in Table.V.

Before closing this section, we comment on the case of $p4g$, which also realizes a unique electromagnetic response at the \bar{M} point. Although different irreps coexist in the magnetic response, one of them exhibits a magnetic response with high multipolarity. If the irrep of \mathcal{O}_{-} is A_1 or B_1 , $g_{-}(\mathbf{B})$ is of the form:

$$g_{p4g-}^{A_1}(\mathbf{B}) = c_{5-} B_x B_y B_z (B_x^2 - B_y^2), \quad (104)$$

$$g_{p4g-}^{B_1}(\mathbf{B}) = c_{3-} B_x B_y B_z, \quad (105)$$

which indicate the magnetic 32-pole and octupole responses, respectively. Similarly, when the irrep of \mathcal{O}_{+} is A_2 , one of electric responses exhibits a 16-pole response,

$$f_{p4g}^{A_2}(\mathbf{E}) = c_{4+} E_x E_y (E_x^2 - E_y^2), \quad (106)$$

$$g_{p4g+}^{A_2}(\mathbf{B}) = c_{4+} B_x B_y (B_x^2 - B_y^2). \quad (107)$$

VII. SUMMARY

Applying the Wigner's test to the identification of 1d topological invariants and establishing the multipole theory for MKPs, we classified the possible magnetic structures for MKPs under the wallpaper groups. For a single MKP, irreps of magnetic structures are classified into the magnetic dipole or octupole and one-to-one correspond to those of gap functions in TSCs. Although almost magnetic structures belong to the magnetic dipole, the magnetic octupole response is realized in two ways: one is the threefold-rotation-symmetry-induced magnetic octupole in spin 3/2 TSCs, which is realized for $p6$, $p3m1$,

$p31m$ and $p6m$. The magnetic response preserves the sixfold rotation symmetry as shown in Fig. 1 (c) and its shape is described by Eq. (77) or (81). The other is the glide-symmetry-induced magnetic octupole in non-symmorphic TSCs, which is realized for pmg and pgg at the BZ boundary. The shape of the magnetic response is given by Eq. (85) as shown in Fig. 2 (c). In addition, we found that two MKPs arise at the \bar{M} point when the surface BZ preserves pgg or $p4g$. The two MKPs potentially exhibit electric multipole responses, which will be discussed somewhere.

Finally, we comment on the possible experimental method for detecting the magnetic structures of a single MKP. Our results predict that the spin structure of the MKPs is anisotropic, so we are able to measure the anisotropy through surface-spin-sensitive measurements, such as spin-resolved tunneling spectroscopy [97, 98], spin relaxation rate [69], spin susceptibility [70], thermal conductivity [99–101] under magnetic fields, and so on. As an example, we discuss the behavior of tunneling conductance under a magnetic field or with a magnet attached, where we assume that only the Zeeman magnetic field affects the MKP. We note that the orbital magnetization is also useful to measure the topological surface states on TSCs [114–119]. Tunnel conductance detects the MKP as a zero bias conductance peak [43]. When the magnetic field is turned on, the MKP shifts from the zero energy, resulting in broadening or splitting of the zero bias conductance peak. When the magnetic structure is the dipole type, such suppression of the zero bias conductance peak can be observed when applying the magnetic field in a specific direction, e.g. a rotation symmetry axis. On the other hand, when the magnetic structure is the octupole type, the suppression occurs in different three directions due to three or sixfold rotation symmetry. Thus, if we apply the in-plane rotating magnetic

field, the recovery of the peak may appear along with sixfold periodicity according to Eq. (77) or (81).

ACKNOWLEDGMENTS

This work was supported by JSPS KAKENHI (Grants Nos. JP18H04224, JP19K14612, JP20H00131, JP20K03835, and JP20H04635), the Sumitomo Foundation (190228), the CREST project (JPMJCR16F2, JPMJCR19T2) from Japan Science and Technology Agency (JST), and the JSPS Core-to-Core Program (A. Advanced Research Network).

Appendix A: Derivation of Eq. (26)

Here we show the derivation of Eq. (26). We start with Eq. (25), which can be rewritten as

$$\begin{aligned}\hat{\gamma}_a &= \int dx \langle u_0^{(a)}(x) | \hat{\Psi}(x) \\ &= \int dx \sum_{i\tau} (u(x)_0^{(a)*})_{i\tau} \hat{\Psi}(x)_{i\tau},\end{aligned}\quad (\text{A1})$$

where i and τ describes internal degrees of freedom for electrons and the Nambu space and the wave function satisfies the commutation relation $\{\hat{\Psi}(x)_{i\tau}, \hat{\Psi}^\dagger(x')_{j\tau'}\} = \delta_{\tau\tau'} \delta_{ij} \delta(x - x')$ and the PHS $\mathcal{C}\hat{\Psi}(x) = \hat{\Psi}(x)$. Similarly, $\hat{\gamma}_a^\dagger$ is given by

$$\hat{\gamma}_a^\dagger = \int dx \langle u_0^{(a)*}(x) | \hat{\Psi}(x)^\dagger. \quad (\text{A2})$$

Then, the commutation relation between $\hat{\gamma}_a$ and $\hat{\gamma}_b^\dagger$ is calculated as

$$\begin{aligned}\{\gamma_a, \gamma_b^\dagger\} &= \int dx dx' \left\{ \langle u_0^{(a)}(x) | \hat{\Psi}(x), \langle u_0^{(b)*}(x') | \hat{\Psi}(x')^\dagger \right\} \\ &= \int dx dx' \sum_{ij} \sum_{\tau\tau'} (u(x)_0^{(a)*})_{i\tau} (u(x')_0^{(b)})_{j\tau'} \\ &\quad \times \left\{ \hat{\Psi}(x)_{i\tau}, \hat{\Psi}(x')_{j\tau'}^\dagger \right\} \\ &= \int dx \sum_{i\tau} (u(x)_0^{(a)*})_{i\tau} (u(x)_0^{(b)})_{i\tau} \\ &= \delta_{ab}\end{aligned}\quad (\text{A3})$$

Also, from Eq. (A2), we find the relation between γ_a and γ_a^\dagger :

$$\begin{aligned}\gamma_a^\dagger &= \int dx \langle u_0^{(a)*}(x) | \tau_x \tau_x \hat{\Psi}(x)^\dagger \\ &= \int dx \langle \mathcal{C}u_0^{(a)}(x) | \hat{\Psi}(x) \\ &= \sum_b \gamma_b C_{ba}^*,\end{aligned}\quad (\text{A4})$$

where we define a unitary matrix $C_{ba} = \langle u_0^{(b)} | \mathcal{C}u_0^{(a)} \rangle = C_{ab}$. Using Eqs. (A3) and (A4), Eq. (A3) is recast into

$$\begin{aligned}\{\gamma_a, \gamma_b^\dagger\} &= \{\gamma_a, \gamma_c\} C_{cb}^* \\ &= \delta_{ab},\end{aligned}\quad (\text{A5})$$

where C_{ab} satisfies

$$C_{ab}^{-1} = C_{ab}^\dagger = C_{ba}^* = C_{ab}^*, \quad (\text{A6})$$

so we obtain

$$\{\gamma_a, \gamma_b\} = C_{ab}. \quad (\text{A7})$$

Appendix B: Derivation of Eq.(53)

In this section, we derive Eq.(53). First, we show the relation

$$\mathcal{T}\rho^{(ab)\dagger}\mathcal{T}^{-1} = -\Gamma\rho^{(ab)}\Gamma^\dagger, \quad \Gamma = -i\mathcal{C}\mathcal{T}. \quad (\text{B1})$$

To show this, we rewrite the left hand side of the above equation as follows,

$$\begin{aligned}\mathcal{T}\rho^{(ab)\dagger}\mathcal{T}^{-1} &= \mathcal{U}_T \left\{ [|u_0^{(a)}\rangle \langle \mathcal{C}u_0^{(b)}| - |u_0^{(b)}\rangle \langle \mathcal{C}u_0^{(a)}|]^\dagger \right\}^* \mathcal{U}_T^\dagger \\ &= \mathcal{U}_T \left[|\mathcal{C}u_0^{(b)}\rangle \langle u_0^{(a)}| - |\mathcal{C}u_0^{(a)}\rangle \langle u_0^{(b)}| \right]^* \mathcal{U}_T^\dagger \\ &= |\mathcal{T}\mathcal{C}u_0^{(b)}\rangle \langle \mathcal{T}u_0^{(a)}| - |\mathcal{T}\mathcal{C}u_0^{(a)}\rangle \langle \mathcal{T}u_0^{(b)}|. \\ &= |\mathcal{T}\mathcal{C}u_0^{(b)}\rangle \langle \mathcal{T}\mathcal{C}\mathcal{C}u_0^{(a)}| - |\mathcal{T}\mathcal{C}u_0^{(a)}\rangle \langle \mathcal{T}\mathcal{C}\mathcal{C}u_0^{(b)}|. \end{aligned}\quad (\text{B2})$$

Then, using $\mathcal{T}\mathcal{C}|u_0^{(a)}\rangle = i\Gamma|u_0^{(a)}\rangle$ and $\mathcal{T}\mathcal{C}\mathcal{C}|u_0^{(a)}\rangle = i\Gamma|\mathcal{C}u_0^{(a)}\rangle$, we obtain Eq. (B1).

Since Γ anticommutes with the BdG Hamiltonian, if $|u_0^{(a)}\rangle$ is a zero mode, $\Gamma|u_0^{(a)}\rangle$ is also a zero mode. Thus, it can be written as

$$\Gamma|u_0^{(a)}\rangle = \sum_b |u_0^{(b)}\rangle [\Gamma_\gamma]_{ba} \quad (\text{B3})$$

with $[\Gamma_\gamma]_{ba} = \langle u_0^{(b)} | \Gamma | u_0^{(a)} \rangle$. From $\{\Gamma, \mathcal{C}\} = 0$, we also have

$$\Gamma|\mathcal{C}u_0^{(a)}\rangle = -\sum_b |\mathcal{C}u_0^{(b)}\rangle [\Gamma_\gamma]_{ba}^* \quad (\text{B4})$$

Therefore, the right hand side of Eq.(B1) is recast into

$$-\Gamma\rho^{(ab)}\Gamma^\dagger = \sum_{cd} \rho^{(cd)} [\Gamma_\gamma]_{ca} [\Gamma_\gamma]_{db}. \quad (\text{B5})$$

Thus, $\rho_\pm^{(ab)}$ in Eq.(44) is rewritten as

$$\begin{aligned}\rho_\pm^{(ab)} &= \frac{1}{2}(\rho^{(ab)} \mp \Gamma\rho^{(ab)}\Gamma^\dagger) \\ &= \sum_{cd} \rho^{(cd)} P_{(cd)(ab)}^\pm\end{aligned}\quad (\text{B6})$$

where $P_{(cd)(ab)}^\pm$ is defined by

$$P_{(cd)(ab)}^\pm = \frac{1}{2}(\delta_{ca}\delta_{db} \pm [\Gamma_\gamma]_{ca}[\Gamma_\gamma]_{db}). \quad (\text{B7})$$

Here we find that $P_{(cd)(ab)}^\pm$ is a projection; it obeys

$$\begin{aligned} P_{(cd)(ab)}^+ + P_{(cd)(ab)}^- &= \delta_{ca}\delta_{db}, \\ \sum_{cd} P_{(ef)(cd)}^\pm P_{(cd)(ab)}^\pm &= P_{(ef)(ab)}^\pm. \end{aligned} \quad (\text{B8})$$

Thus, we also have

$$\rho_\pm^{(ab)} = \sum_{cd} \rho_\pm^{(cd)} P_{(cd)(ab)}^\pm. \quad (\text{B9})$$

Now we derive Eq.(53). Using the relation $\mathcal{U}_g^k \Gamma = \eta_g \Gamma \mathcal{U}_g^k$ and Eqs.(B1) and (38), we find

$$\begin{aligned} \mathcal{U}_g^k \rho_\pm^{(ab)} \mathcal{U}_g^{k\dagger} &= \frac{1}{2} \left(\mathcal{U}_g^k \rho^{(ab)} \mathcal{U}_g^{k\dagger} \pm \Gamma \mathcal{U}_g^k \rho^{(ab)} \mathcal{U}_g^{k\dagger} \Gamma^\dagger \right) \\ &= \sum_{cd} \frac{1}{2} (\rho^{(cd)} \mp \Gamma \rho^{(cd)} \Gamma^\dagger) [\Omega_g]_{(cd)(ab)} \\ &= \sum_{cd} \rho_\pm^{(cd)} [\Omega_g]_{(cd)(ab)}. \end{aligned} \quad (\text{B10})$$

From Eq.(B9), the above equation is recast into

$$\mathcal{U}_g^k \rho_\pm^{(ab)} \mathcal{U}_g^{k\dagger} = \sum_{ef} \rho_\pm^{(ef)} P_{(ef)(cd)}^\pm [\Omega_g]_{(cd)(ab)}, \quad (\text{B11})$$

which is nothing but Eq. (53) because it holds that

$$\sum_{cd} P_{(ef)(cd)}^\pm [\Omega_g]_{(cd)(ab)} = [\Omega_g^\pm]_{(ef)(ab)}. \quad (\text{B12})$$

Appendix C: Double-valued representation of nonsymmorphic wallpaper groups at the BZ boundary

The double-valued representation of nonsymmorphic wallpaper groups is listed in Table VI.

Appendix D: Representation of $f_\pm(\mathbf{B})$ and $g(\mathbf{E})$

Symmetry adopted $f_\pm(\mathbf{B})$ and $g(\mathbf{E})$ are summarized in Tables VII, VIII and IX.

Appendix E: Topological invariants

We here summarize topological invariants associated with the EAZ class. On a high symmetry point \mathbf{k} (a high symmetry line $l_{\mathbf{k}}$), (anti)unitary operators and the BdG Hamiltonian are decomposed into irreps of $G_0^{\mathbf{k}}$ as Eqs. (14) and (15). Then each subsector of the BdG

TABLE VI. Double-valued irreps of nonsymmorphic wallpaper groups at the BZ boundary. In $p4g$, only a minimal set of symmetry operators is shown.

$pg \bar{X}$ point				
	$\{e \mathbf{0}\}$	$\{\sigma_{(010)} \tau_x\}$		
X_1	1	1		
X_2	1	-1		

$pmg \bar{X}$ point				
	$\{e \mathbf{0}\}$	$\{2_z \mathbf{0}\}$	$\{\sigma_{(010)} \tau_x\}$	$\{\sigma_{(100)} \tau_x\}$
X'_1	1	$-i$	1	$-i$
X'_2	1	i	1	i
X'_3	1	i	-1	$-i$
X'_4	1	$-i$	-1	i

$pgg \bar{M}$ point				
	$\{e \mathbf{0}\}$	$\{2_z \mathbf{0}\}$	$\{\sigma_{(010)} \tau_x + \tau_y\}$	$\{\sigma_{(100)} \tau_x + \tau_y\}$
M	σ_0	$-i\sigma_y$	σ_x	σ_z

$p4g \bar{M}$ point ^a				
	$\{e \mathbf{0}\}$	$\{4_z \mathbf{0}\}$	$\{2_z \mathbf{0}\}$	$\{\sigma_{(100)} \tau_x + \tau_y\}$
M_1	σ_0	$e^{\frac{i\pi}{4}(2\sigma_0 + \sigma_z)}$	$-i\sigma_z$	σ_x
M_2	σ_0	$e^{-\frac{i\pi}{4}(2\sigma_0 + \sigma_z)}$	$i\sigma_z$	σ_x

^a Note that the basis used here is slightly different from that shown in the Bilbao Crystallographic Server [110], $P4bm$ (SG# 100), for a sake of convenience. The two bases are transformed to each other under a unitary transformation.

Hamiltonian belongs to the EAZ class and the corresponding topological invariants are defined by using PHS, TRS, and CS projected onto the subsectors. In the following, we define all crystalline symmetry-protected 1d topological invariants explicitly.

1. n -fold rotation symmetry-protected 1d winding number

Firstly, we define the 1d winding number associated with n -fold rotation symmetry ($n = 2, 3, 4, 6$). To see this, we assume that the BdG Hamiltonian is invariant under $\mathcal{U}_{\{n_z|\mathbf{0}\}}$ that satisfies $\mathcal{U}_{\{n_z|\mathbf{0}\}}^n = -\mathbf{1}$ and $[\mathcal{U}_{\{n_z|\mathbf{0}\}}, \mathcal{T}] = [\mathcal{U}_{\{n_z|\mathbf{0}\}}, \mathcal{C}] = 0$. In this case, the BdG Hamiltonian in the subsectors of $\mathcal{U}_{\{n_z|\mathbf{0}\}}$ belong to the class AIII; namely, we have an emergent CS Γ^α within the subsectors. Thus, using $H^\alpha(k)$ and Γ^α , the n -fold rotation symmetry-protected 1d winding number is defined as [7, 72, 74, 120, 121]

$$w_{\text{nR}}^\alpha \equiv \frac{i}{4\pi} \int_{-\pi}^{\pi} dk \text{tr} [\Gamma^\alpha H^\alpha(k)^{-1} \partial_k H^\alpha(k)], \quad (\text{E1})$$

TABLE VII. $g_-(\mathbf{B})$ for 2d point groups, and multipole orders. For C_n and C_{nv} , we choose the rotation axis as the z axis. For C_s , the mirror plane is normal to the z axis.

G_0	IR	$g_-(\mathbf{B})$	multipole order
C_2	A	B_z	Dipole
	B	B_x, B_y	Dipole
C_3	A	B_z	Dipole
	E	$\{B_x, B_y\}$	Dipole
C_4	A	B_z	Dipole
	B	$B_z(B_x^2 - B_y^2), B_y B_y B_z$	Octupole
	E	$\{B_x, B_y\}$	Dipole
C_6	A	B_z	Dipole
	B	$B_x^3 - 3B_x B_y^2, B_y^3 - 3B_y B_x^2$	Octupole
	E ₁	$\{B_z(B_x^2 - B_y^2), B_y B_y B_z\}$	Octupole
	E ₂	$\{B_x, B_y\}$	Dipole
C_s	A	B_z	Dipole
	B	B_x, B_y	Dipole
C_{2v}	A ₁	$B_x B_y B_z$	Octupole
	A ₂	B_z	Dipole
	B ₁	B_y	Dipole
	B ₂	B_x	Dipole
C_{3v}	A ₁	$B_x^3 - 3B_x B_y^2$	Octupole
	A ₂	B_z	Dipole
	E	$\{B_x, B_y\}$	Dipole
C_{4v}	A ₁	$B_x B_y B_z(B_x^2 - B_y^2)$	32-pole
	A ₂	B_z	Dipole
	B ₁	$B_x B_y B_z$	Octupole
	B ₂	$B_z(B_x^2 - B_y^2)$	Octupole
	E	$\{B_x, B_y\}$	Dipole
C_{6v}	A ₁	$B_z(B_x^3 - 3B_x B_y^2)(B_y^3 - 3B_y B_x^2)$	128-pole
	A ₂	B_z	Dipole
	B ₁	$B_y^3 - 3B_y B_x^2$	Octupole
	B ₂	$B_x^3 - 3B_x B_y^2$	Octupole
	E ₁	$\{B_x, B_y\}$	Dipole
	E ₂	$\{B_z(B_x^2 - B_y^2), B_y B_y B_z\}$	Octupole

TABLE VIII. $f(\mathbf{E})$ for C_{2v} and C_{4v} , and multipole orders. We choose the rotation axis as the z axis.

G_0	IR	$f(\mathbf{E})$	multipole order
C_{2v}	A ₁	E_z	Dipole
	A ₂	$E_x E_y$	Quadrupole
	B ₁	E_x	Dipole
	B ₂	E_y	Dipole
C_{4v}	A ₁	E_z	Dipole
	A ₂	$E_x E_y(E_x^2 - E_y^2)$	16-pole
	B ₁	$E_x^2 - E_y^2$	Quadrupole
	B ₂	$E_x E_y$	Quadrupole
	E	(E_x, E_y)	Dipole

TABLE IX. $g_+(\mathbf{B})$ for C_{2v} and C_{4v} , and multipole orders. We choose the rotation axis as the z axis.

G_0	IR	$g_+(\mathbf{B})$	multipole order
C_{2v}	A_1	B_x^2, B_y^2, B_z^2	Quadrupole
	A_2	$B_x B_y$	Quadrupole
	B_1	$B_x B_z$	Quadrupole
	B_2	$B_y B_z$	Quadrupole
C_{4v}	A_1	$B_z^2, B_x^2 + B_y^2$	Quadrupole
	A_2	$B_x B_y (B_x^2 - B_y^2)$	16-pole
	B_1	$B_x^2 - B_y^2$	Quadrupole
	B_2	$B_x B_y$	Quadrupole
	E	$(B_x B_z, B_y B_z)$	Quadrupole

where α labels the subsectors of $\mathcal{U}_{\{n_z|\mathbf{0}\}}$. Equation (E1) appears in the wallpaper groups: $p2$, $p3$, $p4$, $p6$, pm , $p31m$, $p3m1$, $p4m$, $p6m$, pg , pmg , cm and $p4g$. At the \bar{M} point in the surface BZ, the 4-fold rotation symmetry in $p4g$ leads to $w_{4R}^{\alpha_0} = -w_{4R}^{\alpha_1} = w_{4R}^{\alpha_2} = -w_{4R}^{\alpha_3}$ for the A₁ gap functions and $w_{4R}^{\alpha_0} = -w_{4R}^{\alpha_1} = -w_{4R}^{\alpha_2} = w_{4R}^{\alpha_3}$ for the A₂ gap functions due to TRS and the glide symmetry, where $\alpha_m = \exp[i\pi(2m+1)/4]$ is an eigenvalue of $\mathcal{U}_{\{4_z|\mathbf{0}\}}$. Therefore, Majorana zero modes appear as a quartet consisting of two MKPs.

2. Mirror-reflection-symmetry-protected 1d winding number

Secondly, we define the 1d winding number associated with mirror-reflection symmetry $\{\sigma|\mathbf{0}\}$, which is defined in a similar way to the n -fold-rotation-symmetry protected 1d winding number. When $\mathcal{U}_{\{\sigma|\mathbf{0}\}}$ commutes with the BdG Hamiltonian, PHS, and TRS, the EAZ class of BdG Hamiltonian is in class AIII. Hence the mirror-reflection-symmetry-protected 1d winding number is described as

$$w_\sigma^\alpha \equiv \frac{i}{4\pi} \int_{-\pi}^{\pi} dk \operatorname{tr} [\Gamma^\alpha H^\alpha(k)^{-1} \partial_k H^\alpha(k)], \quad (\text{E2})$$

where α is an eigenvalue of $\mathcal{U}_{\{\sigma|\mathbf{0}\}}$. The 1d winding number appears in the wallpaper groups: pm , pm , $p31m$, $p3m1$, $p6m$, pg , cm , pmg , cm , and pgg .

3. n -fold rotation symmetry-protected 1d \mathbb{Z}_2 invariant

Thirdly, we find n -fold rotation symmetry-protected 1d \mathbb{Z}_2 invariant in the wallpaper groups: $p2$, $p3$, $p6$, and $p4g$. We define them case by case. For $p2$, the EAZ class of the subsectors of $\mathcal{U}_{\{2_z|\mathbf{0}\}}$ is D when the irrep of gap functions is B. We have an emergent PHS within the subsectors and a 1d \mathbb{Z}_2 invariant associated with the emergent PHS.

Using the Berry connection in terms of eigenstates of $H^\alpha(k)$, $|u_{n,k}^\alpha\rangle$, the 1d \mathbb{Z}_2 invariant is defined by

$$\nu_{2R}^\alpha \equiv \frac{1}{\pi} \int_{-\pi}^{\pi} dk \mathcal{A}^\alpha(k) \mod 2, \quad (\text{E3})$$

with

$$\mathcal{A}^\alpha(k) = -i \sum_{n \in \text{occ}} \langle u_{n,k}^\alpha | \partial_k | u_{n,k}^\alpha \rangle, \quad (\text{E4})$$

where α is an eigenvalue of $\mathcal{U}_{\{2_z|\mathbf{0}\}}$ and the summation is taken over the occupied state with a fixed α . $\nu_{2R}^\alpha = -\nu_{2R}^{-\alpha}$ is satisfied due to TRS.

For $p3$ and $p6$, a 1d \mathbb{Z}_2 invariant exists only when the spin of electrons is $3/2$. The 3-fold rotation operator $\mathcal{U}_{\{3_z|\mathbf{0}\}}$ has a real eigenvalue and always commutes with \mathcal{T} and \mathcal{C} , so that the subsector of $\mathcal{U}_{\{3_z|\mathbf{0}\}}$ belongs to class DIII. The 1d \mathbb{Z}_2 invariant ν_{3R}^α is defined by

$$\nu_{3R}^\alpha = \frac{1}{2\pi} \int_{-\pi}^{\pi} dk \mathcal{A}^\alpha(k) \mod 2, \quad (\text{E5})$$

where the basis of \mathcal{A}^α is an eigenstate of $\mathcal{U}_{\{3_z|\mathbf{0}\}}$ and the gauge fixing condition $\mathcal{T}|u_{2n-1,k}^\alpha\rangle = |u_{2n,-k}^\alpha\rangle$ is imposed. Similarly, the 6-fold rotation operator $\mathcal{U}_{\{6_z|\mathbf{0}\}}$ satisfies $\mathcal{U}_{\{6_z|\mathbf{0}\}}^2 = -1$ and $\{\mathcal{U}_{\{6_z|\mathbf{0}\}}, \mathcal{C}\} = 0$, when the spin of electrons is $3/2$ and the irrep of gap function is B. Thus, the subsectors of $\mathcal{U}_{\{6_z|\mathbf{0}\}}$ belongs to class D, so the 1d \mathbb{Z}_2 invariant ν_{6R}^α is defined by Eq. (E3), where α is an eigenvalue of $\mathcal{U}_{\{6_z|\mathbf{0}\}}$.

On the other hand, for $p4g$, a glide symmetry plays an important role. A 1d \mathbb{Z}_2 invariant is defined at the \bar{M} point of $p4g$ when the irrep of the gap function is B_1 . Here $p4g$ consists of the 4-fold rotation operator $\{4_z|\mathbf{0}\}$ and the glide operator $\{\sigma_{(010)}|\tau_x + \tau_y\}$. For the B_1 gap function, the PH operator satisfies $\{\mathcal{U}_{\{4_z|\mathbf{0}\}}, \mathcal{C}\} = [\mathcal{U}_{\{\sigma_{(010)}|\tau_x + \tau_y\}}, \mathcal{C}] = 0$. Thus, there is an emergent PHS operator $\mathcal{C}' = \mathcal{C}\mathcal{U}_{\{\sigma_{(010)}|\tau_x + \tau_y\}}$ with $(\mathcal{C}')^2 = 1$ for each subsector of $\{4_z|\mathbf{0}\}$, resulting in that the EAZ class is D. Therefore, the 1d \mathbb{Z}_2 invariant ν_{4R}^α is defined in a similar manner to Eq. (E3), where the basis of \mathcal{A}^α is an eigenstate of $\mathcal{U}_{\{4_z|\mathbf{0}\}}$. Moreover, TRS and the other SG operators impose additional constraints on ν_{4R}^α , which leads to $\nu_{4R}^{\alpha_0} = \nu_{4R}^{\alpha_1} = -\nu_{4R}^{\alpha_2} = -\nu_{4R}^{\alpha_3}$, i.e., two MKPs appears.

4. Mirror-reflection symmetry-protected 1d \mathbb{Z}_2 invariant

Fourthly, we find a 1d \mathbb{Z}_2 invariant associated with mirror-reflection symmetry $\{\sigma|\mathbf{0}\}$, which is defined in a similar way to the n -fold rotation symmetry-protected 1d \mathbb{Z}_2 invariant. When $\mathcal{U}_{\{\sigma|\mathbf{0}\}}$ anticommutes with PHS, the EAZ class of the subsectors becomes class D. That is to say, the mirror-reflection symmetry-protected 1d \mathbb{Z}_2 invariant ν_σ^α is given by Eq. (E3) in terms of $\mathcal{A}^\alpha(k)$ in the subsectors of $\mathcal{U}_{\{\sigma|\mathbf{0}\}}$. The 1d \mathbb{Z}_2 appears in the wallpaper groups: pm , $p31m$, $p3m1$, pg , cm , and pmg .

5. Glide symmetry-protected 1d \mathbb{Z}_2 invariant

Finally, we define the glide symmetry-protected 1d \mathbb{Z}_2 invariant [9, 112]. To show this, we consider $pg = \{\{e|\mathbf{0}\}, \{\sigma_{(010)}|\tau_x\}\}$, where $\sigma_{(010)}$ is the mirror reflection with respect to the (010) plane and τ_x is a half translation in the x direction. At the \bar{X} point or the \bar{M} point in the surface BZ, a nontrivial factor system arises as $z_{\{\sigma_{(010)}|\tau_x\}, \{\sigma_{(010)}|\tau_x\}} = 1$, so the glide operator satisfies $\mathcal{U}_{\{\sigma_{(010)}|\tau_x\}}^2 = 1$ and its eigenvalue is real. When the BdG Hamiltonian is invariant under $\mathcal{U}_{\{\sigma_{(010)}|\tau_x\}}$ and the irrep of the gap function is A, we can define the following 1d topological invariant at $k_x = \pi$: As $[\mathcal{U}_{\{\sigma_{(010)}|\tau_x\}}, \mathcal{C}] = [\mathcal{U}_{\{\sigma_{(010)}|\tau_x\}}, \mathcal{T}] = 0$, PHS and TRS are retained in the subsector of $\mathcal{U}_{\{\sigma_{(010)}|\tau_x\}}$ and thus the EAZ class is DIII. The glide symmetry-protected 1d \mathbb{Z}_2 invariant is defined as

$$\nu_G^\alpha = \frac{1}{2\pi} \int_{-\pi}^{\pi} dk \mathcal{A}^\alpha(k) \mod 2, \quad (\text{E6})$$

where $|u_{n,k}^\alpha\rangle_\pm$ is an eigenstate of $\mathcal{U}_{\{\sigma_y|\tau_x\}}$ and the gauge fixing condition $\mathcal{T}|u_{2n-1,k}^\alpha\rangle_\pm = |u_{2n,-k}^\alpha\rangle_\pm$ is imposed. The \mathbb{Z}_2 invariant in Eq. (E6) appears in the wallpaper groups: pg and pgg . For the \bar{M} point of pgg , we have an additional SG operator anticommute with the glide operator, which yields $\nu_{G1D}^\alpha = \nu_{G1D}^{-\alpha}$ and thus two MKPs appear there.

Appendix F: Enhancement of rotational symmetry

We show here the enhancement of rotational symmetry. We start with a time-reversal invariant effective Hamiltonian for spin j_z electrons. Because of TRS, the Hamiltonian minimally consists of spin $\pm j_z$ electrons, and thus it is given by a 2×2 matrix

$$\begin{aligned} H(\mathbf{k}) &= a_0(\mathbf{k})s_0 + a_x(\mathbf{k})s_x + a_y(\mathbf{k})s_y + a_z(\mathbf{k})s_z \\ &= a_0(\mathbf{k})s_0 + a_-(\mathbf{k})s_+ + a_+(\mathbf{k})s_- + a_z(\mathbf{k})s_z, \end{aligned} \quad (\text{F1})$$

where s_i are the Pauli matrices acting on the spin space ($|j_z\rangle, |-j_z\rangle$), $a_i(\mathbf{k})$ are real functions of \mathbf{k} , and $a_\pm = a_x \pm ia_y$ and $s_\pm = (s_x \pm is_y)/2$.

Then, let us assume that the Hamiltonian in Eq. (F1) is invariant under the n -fold rotation $\{n_z|\mathbf{0}\}$ with respect to the z axis:

$$U_{\{n_z|\mathbf{0}\}} H(\mathbf{k}) U_{\{n_z|\mathbf{0}\}}^\dagger = H(\{n_z|\mathbf{0}\}\mathbf{k}), \quad (\text{F2})$$

where $\{n_z|\mathbf{0}\}\mathbf{k} = (e^{i2\pi/n}k_+, e^{-i2\pi/n}k_-, k_z)$ and $U_{\{n_z|\mathbf{0}\}}$ is of the form:

$$U_{\{n_z|\mathbf{0}\}} = \text{diag}(e^{-i\frac{2\pi}{n}j_z}, e^{i\frac{2\pi}{n}j_z}). \quad (\text{F3})$$

In order for Eq. (F1) to satisfy Eq. (F2), each coefficient

in Eq. (F1) should satisfy

$$a_0(\mathbf{k}) = a_0(\{n_z|\mathbf{0}\}\mathbf{k}), \quad (\text{F4a})$$

$$e^{-i\frac{4\pi}{n}j_z}a_-(\mathbf{k}) = a_-(\{n_z|\mathbf{0}\}\mathbf{k}), \quad (\text{F4b})$$

$$e^{i\frac{4\pi}{n}j_z}a_+(\mathbf{k}) = a_+(\{n_z|\mathbf{0}\}\mathbf{k}), \quad (\text{F4c})$$

$$a_z(\mathbf{k}) = a_z(\{n_z|\mathbf{0}\}\mathbf{k}). \quad (\text{F4d})$$

Thus, if $e^{i4\pi j_z/n} \neq 1$, a_+ and a_- vanish at the high symmetry line $(0, 0, k_z)$. This implies that at the high symmetry line, the n -fold rotation symmetry becomes the continuous rotation one, and the Hamiltonian is invariant under any rotation with respect to the z -direction,

$$U_\theta H(0, 0, k_z) U_\theta^\dagger = H(0, 0, k_z), \quad (\text{F5})$$

where $U_\theta = \text{diag}(e^{-i\theta j_z}, e^{i\theta j_z})$ ($0 \leq \theta < 2\pi$). For $j_z = 1/2$ and $j_z = 5/2$, the condition $e^{i4\pi j_z/n} \neq 1$ is met for any $n = 2, 3, 4, 6$, and thus the enhancement of rotation symmetry in the above always occurs. On the other hand, for $j_z = 3/2$, the condition is met only for $n = 2, 4, 6$. The enhancement of rotation symmetry does not occur for $j_z = 3/2$ with $n = 3$.

The enhancement of rotation symmetry may provide an additional protection for MKPs. For instance, let us consider a topological superconductor hosting a MKP on a surface with 3-fold rotation symmetry. In the presence of a finite magnetic field parallel to the surface, the 3-fold rotation symmetry is explicitly broken, but if the system consists of $j_z = 1/2$ or $j_z = 5/2$ electrons, we may retain an additional symmetry: By combining 2-fold rotation symmetry obtained by the symmetry enhancement with TRS, the system supports magnetic 2-fold rotation symmetry. The magnetic rotation symmetry may stabilize the surface MKP [72]. Such stabilization is expected for a MKP on the (111) surface of superconducting topological insulator $\text{Cu}_x\text{Bi}_2\text{Se}_3$ with the A_{1u} gap function [52].

Appendix G: Superconducting nodes and Majorana multipole response

In our theory, we implicitly assume that there is no node on the high symmetry line $l_{\mathbf{k}}$ in the bulk BZ where the 1d topological invariant is defined. In the following, we show the topological classification for superconducting nodes, which is performed in a similar manner to the topological classification of 1d topological invariants, and discuss when this assumption is satisfied. In topological arguments, a stable node on $l_{\mathbf{k}}$ is classified by a 0d topological invariant. The possible 0d topological invariant is specified by the Wigner's test in Eqs. (16), (17), and (18), where only symmetries that keep a position of the node are taken into account.

In the following, we classify possible nodes on the high symmetry line for systems (i) without and (ii) with spatial inversion symmetry, respectively. The results are summarized in Table X, where possible 0d topological

invariants under the wallpaper groups are classified in superconductors without spatial inversion symmetry, even-parity superconductors, and odd-parity superconductors.

(i) *systems without inversion symmetry.* – In addition to $G_0^{\mathbf{k}}$, we need to consider CS, both of which keep any point on $l_{\mathbf{k}}$ invariant. The total group we consider is

$$G_0^{\mathbf{k}} + \Gamma G_0^{\mathbf{k}}, \quad (\text{G1})$$

which implies that the Wigner's test is determined solely by W_α^Γ in Eq. (18). By forgetting W_α^T and W_α^C , the emergent AIII, BDI, DIII, CI, and CII classes in Tables II and III change to the emergent AIII class. In these cases, no 0d topological invariant exists, and thus the system on $l_{\mathbf{k}}$ is fully gapped in general. On the other hand, the emergent A, AI, AII, D, and C classes in Tables II and III change to the A class. As the A class hosts a 0d topological invariant, the latter emergent classes may have a stable node on $l_{\mathbf{k}}$. Among these emergent classes, only the D class has a 1d topological invariant at the same time.

(ii) *systems with inversion symmetry.* – Next, we take into account spatial inversion $\{I|\mathbf{0}\}$. Combining TRS and PHS with space inversion, we have $\mathfrak{C} \equiv \{I|\mathbf{0}\}C$ and $\mathfrak{T} \equiv \{I|\mathbf{0}\}T$, respectively, both of which keep any point on $l_{\mathbf{k}}$ invariant. The total group relevant to the node stability is

$$G_0^{\mathbf{k}} + \mathfrak{T}G_0^{\mathbf{k}} + \mathfrak{C}G_0^{\mathbf{k}} + \Gamma G_0^{\mathbf{k}}, \quad (\text{G2})$$

and the Wigner's test for \mathfrak{T} and \mathfrak{C} is given by [109]

$$W_\alpha^{\mathfrak{T}} \equiv \frac{1}{|G_0|} \sum_{g \in G_0} z_{\mathfrak{T}g, \mathfrak{T}g} \chi[U_{(\mathfrak{T}g)^2}^\alpha] = \pm 1, 0, \quad (\text{G3})$$

$$W_\alpha^{\mathfrak{C}} \equiv \frac{1}{|G_0|} \sum_{g \in G_0} z_{\mathfrak{C}g, \mathfrak{C}g} \chi[U_{(\mathfrak{C}g)^2}^\alpha] = \pm 1, 0, \quad (\text{G4})$$

where $\mathfrak{T}^2 = z_{\mathfrak{T}, \mathfrak{T}} = -1$, $\mathfrak{C}^2 = z_{\mathfrak{C}, \mathfrak{C}} = \eta_I$ and $\eta_I = 1$ (-1) indicates an even (odd) parity gap function. First, we apply the Wigner's test in Eqs. (G3), (G4), and (18) to symmetric wallpaper groups. In these cases, the Wigner's test reads

$$(W_\alpha^{\mathfrak{T}}, W_\alpha^{\mathfrak{C}}, W_\alpha^\Gamma) = (W_\alpha^T, \eta_I W_\alpha^C, W_\alpha^\Gamma), \quad (\text{G5})$$

which determines the EAZ classes for the nodal structure on $l_{\mathbf{k}}$. Note that the EAZ classes are different from those in Tables II and VI only for the odd-parity superconductors.

From this result, we find that the 1d topological invariants on $l_{\mathbf{k}}$ is generally well-defined for odd parity superconductors: The 1d topological invariants can be nonzero when the EAZ in Table II and III is AIII, BDI, D, DIII, or CII classes, and from Eq.(G5), these classes correspond to AIII, CI, C, CII, and DIII, respectively. Because the latter EAZ classes do not have 0d topological invariants, no stable node appear on $l_{\mathbf{k}}$. On the other hand, for even parity superconductors, the emergent BDI class has both

TABLE X. Classification of point nodes under the wallpaper groups. For each table, the first, second, third, and forth columns show irreps of gap functions, emergent Altland Zirnbauer classes for systems without spatial inversion symmetry, with even-parity pairings, and with odd-parity pairings, respectively. Here numbers in parentheses represent 0d topological invariants.

$p1 (C_1)$, spin 1/2				$p2 (C_2)$, spin 1/2				$p3 (C_3)$, spin 1/2			
IR of Δ	w/o IS	even parity	odd parity	IR of Δ	w/o IS	even parity	odd parity	IR of Δ	w/o IS	even parity	odd parity
A	AIII(0)	DIII(0)	CII(0)	A	AIII(0)	AIII(0)	AIII(0)	A	AIII(0)	AIII(0)	AIII(0)
				B	A(\mathbb{Z})	D(\mathbb{Z}_2)	C(0)				
$p3 (C_3)$, spin 3/2				$p4 (C_4)$, spin 1/2 or 3/2				$p6 (C_6)$, spin 1/2 or 5/2			
IR of Δ	w/o IS	even parity	odd parity	IR of Δ	w/o IS	even parity	odd parity	IR of Δ	w/o IS	even parity	odd parity
A	AIII(0)	DIII(0)	CII(0)	A	AIII(0)	AIII(0)	AIII(0)	A	AIII(0)	AIII(0)	AIII(0)
				B	A(\mathbb{Z})	A(\mathbb{Z})	A(\mathbb{Z})	B	A(\mathbb{Z})	A(\mathbb{Z})	A(\mathbb{Z})
$p6 (C_6)$, spin 3/2				$pm (C_s)$, spin 1/2				$pm m (C_{2v})$, spin 1/2			
IR of Δ	w/o IS	even parity	odd parity	IR of Δ	w/o IS	even parity	odd parity	IR of Δ	w/o IS	even parity	odd parity
A	AIII(0)	AIII(0)	AIII(0)	A	AIII(0)	AIII(0)	AIII(0)	A ₁	AIII(0)	CI(0)	BDI(\mathbb{Z}_2)
B	A(\mathbb{Z})	D(\mathbb{Z}_2)	C(0)	B	A(\mathbb{Z})	D(\mathbb{Z}_2)	C(0)	A ₂	AIII(0)	BDI(\mathbb{Z}_2)	CI(0)
								B ₁	AIII(0)	BDI(\mathbb{Z}_2)	CI(0)
								B ₂	AIII(0)	BDI(\mathbb{Z}_2)	CI(0)
$p31m, p3m1 (C_{3v})$, spin 1/2				$p31m, p3m1 (C_{3v})$, spin 3/2				$p4m (C_{4v})$, spin 1/2 or 3/2			
IR of Δ	w/o IS	even parity	odd parity	IR of Δ	w/o IS	even parity	odd parity	IR of Δ	w/o IS	even parity	odd parity
A ₁	AIII(0)	CI(0)	BDI(\mathbb{Z}_2)	A ₁	AIII(0)	AIII(0)	AIII(0)	A ₁	AIII(0)	CI(0)	BDI(\mathbb{Z}_2)
A ₂	AIII(0)	BDI(\mathbb{Z}_2)	CI(0)	A ₂	A(\mathbb{Z})	D(\mathbb{Z}_2)	C(0)	A ₂	AIII(0)	BDI(\mathbb{Z}_2)	CI(0)
								B ₁	A(\mathbb{Z})	AI(\mathbb{Z})	AI(\mathbb{Z})
								B ₂	A(\mathbb{Z})	AI(\mathbb{Z})	AI(\mathbb{Z})
$p6m (C_{6v})$, spin 1/2 or 5/2				$p6m (C_{6v})$, spin 3/2				$pg (C_s) \bar{X}$ point			
IR of Δ	w/o IS	even parity	odd parity	IR of Δ	w/o IS	even parity	odd parity	IR of Δ	w/o IS	even parity	odd parity
A ₁	AIII(0)	CI(0)	BDI(\mathbb{Z}_2)	A ₁	AIII(0)	CI(0)	BDI(\mathbb{Z}_2)	A	AIII(0)	AIII(0)	AIII(0)
A ₂	AIII(0)	BDI(\mathbb{Z}_2)	CI(0)	A ₂	AIII(0)	BDI(\mathbb{Z}_2)	CI(0)	B	A(\mathbb{Z})	D(\mathbb{Z}_2)	C(0)
B ₁	A(\mathbb{Z})	AI(\mathbb{Z})	AI(\mathbb{Z})	B ₁	AIII(0)	BDI(\mathbb{Z}_2)	CI(0)				
B ₂	A(\mathbb{Z})	AI(\mathbb{Z})	AI(\mathbb{Z})	B ₂	AIII(0)	BDI(\mathbb{Z}_2)	CI(0)				
$pmg (C_{2v}) \bar{X}$ point				$pgg (C_{2v}) \bar{M}$ point				$p4g (C_{4v}) \bar{M}$ point			
IR of Δ	w/o IS	even parity	odd parity	IR of Δ	w/o IS	even parity	odd parity	IR of Δ	w/o IS	even parity	odd parity
A ₁	AIII(0)	AIII(0)	AIII(0)	A ₁	AIII(0)	DIII(0)	CII(0)	A ₁	AIII(0)	AIII(0)	AIII(0)
A ₂	A(\mathbb{Z})	A(\mathbb{Z})	A(\mathbb{Z})	A ₂	AIII(0)	CH(0)	DIII(0)	A ₂	AIII(0)	AIII(0)	AIII(0)
B ₁	A(\mathbb{Z})	A(\mathbb{Z})	A(\mathbb{Z})	B ₁	AIII(0)	DIII(0)	CH(0)	B ₁	A(\mathbb{Z})	D(\mathbb{Z}_2)	C(0)
B ₂	A(\mathbb{Z})	D(\mathbb{Z}_2)	C(0)	B ₂	AIII(0)	DIII(0)	CH(0)	B ₂	A(\mathbb{Z})	C(0)	D(\mathbb{Z}_2)

1d and 0d topological invariants. In this case, we need to avoid stable nodes to define the 1d topological invariant.

For nonsymmorphic groups, we need to perform the Wigner's test case by case. First, we consider pg at the \bar{X}

point, which is given by $\{\{e|0\}, \{\sigma_{(010)}|\tau_x\}\}$. We obtain

$$(W_\alpha^\tau, W_\alpha^\epsilon, W_\alpha^\Gamma) = \left(0, \frac{\eta_I}{2}(1 - \eta_{\sigma_{(010)}}), \frac{1}{2}(1 + \eta_{\sigma_{(010)}})\right). \quad (G6)$$

The system has a nontrivial 1d topological invariant for the A gap function ($\eta_{\sigma_{(010)}} = 1$). (See Table VI.) The corresponding EAZ for the node structure is AIII, irre-

spective of η_I . Thus, no point node appears.

For $pmg = \{\{e|0\}, \{2_z|0\}, \{\sigma_{(010)}|\tau_x\}, \{\sigma_{(100)}|\tau_x\}\}$ at

$$(W_\alpha^\tau, W_\alpha^\epsilon, W_\alpha^\Gamma) = \left(0, \frac{\eta_I}{2}(1 - \eta_{2_z} - \eta_{\sigma_{(010)}} + \eta_{\sigma_{(100)}}), \frac{1}{4}(1 + \eta_{2_z} + \eta_{\sigma_{(010)}} + \eta_{\sigma_{(100)}})\right). \quad (G7)$$

In this case, the system has a nontrivial 1d topological invariant for the A_1 gap function ($\eta_{2_z} = \eta_{\sigma_{(010)}} = \eta_{\sigma_{(100)}} = 1$) or the B_1 gap function ($-\eta_{2_z} = \eta_{\sigma_{(010)}} = -\eta_{\sigma_{(100)}} = 1$). The EAZ class for the node structure is AIII (A) for the A_1 (B_1) gap function, regardless of η_I , and thus a stable node appears for the B_1 gap function, which should be avoided to define the 1d topological invariant on l_k . A similar node appears for pgg and $p4g$ at the \bar{X} point.

For $pgg = \{\{e|0\}, \{2_z|0\}, \{\sigma_{(010)}|\tau_x + \tau_y\}, \{\sigma_{(100)}|\tau_x + \tau_y\}\}$ at the \bar{M} point, we have

$$(W_\alpha^\tau, W_\alpha^\epsilon, W_\alpha^\Gamma) = \left(-1, \frac{\eta_I}{2}(1 - \eta_{2_z} + \eta_{\sigma_{(010)}} + \eta_{\sigma_{(100)}}), 1\right). \quad (G8)$$

For any gap function, the EAZ class for the node structure is DIII or CII, and thus no 0d topological invariant exists.

the \bar{X} point, the Wigner's test becomes

Finally, we consider $p4g$ at the \bar{M} point, which is generated by $\{\{2_z|0\}, \{4_z^+|0\}, \{\sigma_{(010)}|\tau_x + \tau_y\}, \{\sigma_{(110)}|\tau_x + \tau_y\}\}$. The Wigner's test is

$$(W_\alpha^\tau, W_\alpha^\epsilon, W_\alpha^\Gamma) = \left(0, \frac{\eta_I}{4}(1 - \eta_{2_z} + 2\eta_{\sigma_{(010)}} - 2\eta_{\sigma_{(110)}}), \frac{1}{8}(4 + 4\eta_{4_z^+})\right). \quad (G9)$$

We have a nontrivial 1d topological invariant for the A_1 ($\eta_{4_z^+} = \eta_{2_z} = \eta_{\sigma_{(010)}} = \eta_{\sigma_{(110)}} = 1$), the A_2 ($\eta_{4_z^+} = \eta_{2_z} = -\eta_{\sigma_{(010)}} = -\eta_{\sigma_{(110)}} = 1$), and the B_1 gap functions ($-\eta_{4_z^+} = \eta_{2_z} = \eta_{\sigma_{(010)}} = -\eta_{\sigma_{(110)}} = 1$). For the A_1 and A_2 gap functions, the EAZ class for the node structure is AIII, and there is no point node. On the other hand, for the B_1 gap function, the EAZ class is D for $\eta_I = 1$ and C for $\eta_I = -1$. Therefore, we can avoid a point node when the parity of the gap function is odd.

-
- [1] A. P. Schnyder, S. Ryu, A. Furusaki, and A. W. W. Ludwig, Classification of topological insulators and superconductors in three spatial dimensions, *Phys. Rev. B* **78**, 195125 (2008).
 - [2] A. Kitaev, Periodic table for topological insulators and superconductors, *AIP Conference Proceedings* **1134**, 22 (2009).
 - [3] A. P. Schnyder, S. Ryu, A. Furusaki, and A. W. W. Ludwig, Classification of topological insulators and superconductors, *AIP Conference Proceedings* **1134**, 10 (2009).
 - [4] S. Ryu, A. P. Schnyder, A. Furusaki, and A. W. W. Ludwig, Topological insulators and superconductors: tenfold way and dimensional hierarchy, *New Journal of Physics* **12**, 065010 (2010).
 - [5] T. Morimoto and A. Furusaki, Topological classification with additional symmetries from clifford algebras, *Phys. Rev. B* **88**, 125129 (2013).
 - [6] C.-K. Chiu, H. Yao, and S. Ryu, Classification of topological insulators and superconductors in the presence of reflection symmetry, *Phys. Rev. B* **88**, 075142 (2013).
 - [7] K. Shiozaki and M. Sato, Topology of crystalline insulators and superconductors, *Phys. Rev. B* **90**, 165114 (2014).
 - [8] K. Shiozaki, M. Sato, and K. Gomi, Z_2 topology in non-symmorphic crystalline insulators: Möbius twist in surface states, *Phys. Rev. B* **91**, 155120 (2015).
 - [9] K. Shiozaki, M. Sato, and K. Gomi, Topology of non-symmorphic crystalline insulators and superconductors, *Phys. Rev. B* **93**, 195413 (2016).
 - [10] C.-K. Chiu, J. C. Y. Teo, A. P. Schnyder, and S. Ryu, Classification of topological quantum matter with symmetries, *Rev. Mod. Phys.* **88**, 035005 (2016).
 - [11] K. Shiozaki, M. Sato, and K. Gomi, Topological crystalline materials: General formulation, module structure, and wallpaper groups, *Phys. Rev. B* **95**, 235425 (2017).
 - [12] C. Fang, B. A. Bernevig, and M. J. Gilbert, Topological crystalline superconductors with linearly and projectively represented C_n symmetry, *arXiv preprint arXiv:1701.01944* (2017).
 - [13] K. Shiozaki, M. Sato, and K. Gomi, Atiyah-Hirzebruch spectral sequence in band topology: General formalism and topological invariants for 230 space groups, *arXiv preprint arXiv:1802.06694* (2018).
 - [14] E. Cornfeld and A. Chapman, Classification of crystalline topological insulators and superconductors with point group symmetries, *Phys. Rev. B* **99**, 075105 (2019).
 - [15] K. Shiozaki, The classification of surface states of topological insulators and superconductors with magnetic point group symmetry, *arXiv preprint arXiv:1907.09354* (2019).
 - [16] N. Okuma, M. Sato, and K. Shiozaki, Topological classification under nonmagnetic and magnetic point group symmetry: Application of real-space Atiyah-Hirzebruch

- spectral sequence to higher-order topology, Phys. Rev. B **99**, 085127 (2019).
- [17] Z. Song, S.-J. Huang, Y. Qi, C. Fang, and M. Hermele, Topological states from topological crystals, Science advances **5**, eaax2007 (2019).
 - [18] B. Bradlyn, L. Elcoro, J. Cano, M. Vergniory, Z. Wang, C. Felser, M. Aroyo, and B. A. Bernevig, Topological quantum chemistry, Nature **547**, 298 (2017).
 - [19] J. Kruthoff, J. de Boer, J. van Wezel, C. L. Kane, and R.-J. Slager, Topological classification of crystalline insulators through band structure combinatorics, Phys. Rev. X **7**, 041069 (2017).
 - [20] H. C. Po, A. Vishwanath, and H. Watanabe, Symmetry-based indicators of band topology in the 230 space groups, Nature communications **8**, 50 (2017).
 - [21] Z. Song, T. Zhang, Z. Fang, and C. Fang, Quantitative mappings between symmetry and topology in solids, Nature communications **9**, 3530 (2018).
 - [22] E. Khalaf, H. C. Po, A. Vishwanath, and H. Watanabe, Symmetry indicators and anomalous surface states of topological crystalline insulators, Phys. Rev. X **8**, 031070 (2018).
 - [23] L. Elcoro, B. J. Wieder, Z. Song, Y. Xu, B. Bradlyn, and B. A. Bernevig, Magnetic topological quantum chemistry, arXiv preprint arXiv:2010.00598 (2020).
 - [24] T. Zhang, Y. Jiang, Z. Song, H. Huang, Y. He, Z. Fang, H. Weng, and C. Fang, Catalogue of topological electronic materials, Nature **566**, 475 (2019).
 - [25] M. Vergniory, L. Elcoro, C. Felser, N. Regnault, B. A. Bernevig, and Z. Wang, A complete catalogue of high-quality topological materials, Nature **566**, 480 (2019).
 - [26] F. Tang, H. C. Po, A. Vishwanath, and X. Wan, Topological materials discovery by large-order symmetry indicators, Science Advances **5**, eaau8725 (2019).
 - [27] F. Tang, H. C. Po, A. Vishwanath, and X. Wan, Efficient topological materials discovery using symmetry indicators, Nature Physics **15**, 470 (2019).
 - [28] D. Wang, F. Tang, J. Ji, W. Zhang, A. Vishwanath, H. C. Po, and X. Wan, Two-dimensional topological materials discovery by symmetry-indicator method, Phys. Rev. B **100**, 195108 (2019).
 - [29] Y. Xu, L. Elcoro, Z.-D. Song, B. J. Wieder, M. Vergniory, N. Regnault, Y. Chen, C. Felser, and B. A. Bernevig, High-throughput calculations of magnetic topological materials, Nature **586**, 702 (2020).
 - [30] S. Ono, Y. Yanase, and H. Watanabe, Symmetry indicators for topological superconductors, Phys. Rev. Research **1**, 013012 (2019).
 - [31] A. Skurativska, T. Neupert, and M. H. Fischer, Atomic limit and inversion-symmetry indicators for topological superconductors, Phys. Rev. Research **2**, 013064 (2020).
 - [32] K. Shiozaki, Variants of the symmetry-based indicator, arXiv preprint arXiv:1907.13632 (2019).
 - [33] M. Geier, P. W. Brouwer, and L. Trifunovic, Symmetry-based indicators for topological Bogoliubov-de Gennes hamiltonians, Phys. Rev. B **101**, 245128 (2020).
 - [34] S. Ono, H. C. Po, and H. Watanabe, Refined symmetry indicators for topological superconductors in all space groups, Science Advances **6**, eaaz8367 (2020).
 - [35] S. Ono, H. C. Po, and K. Shiozaki, \mathbb{Z}_2 -enriched symmetry indicators for topological superconductors in the 1651 magnetic space groups, arXiv preprint arXiv:2008.05499 (2020).
 - [36] C.-R. Hu, Midgap surface states as a novel signature for $d_{x^2-y^2}$ -wave superconductivity, Phys. Rev. Lett. **72**, 1526 (1994).
 - [37] S. Kashiwaya and Y. Tanaka, Tunnelling effects on surface bound states in unconventional superconductors, Rep. Prog. Phys. **63**, 1641 (2000).
 - [38] G. E. Volovik, *The Universe in a Helium Droplet* (Oxford University Press, Oxford, 2003).
 - [39] M. Sato, Topological properties of spin-triplet superconductors and Fermi surface topology in the normal state, Phys. Rev. B **79**, 214526 (2009).
 - [40] F. Wilczek, Majorana returns, Nature Phys. **5**, 614 (2009).
 - [41] M. Z. Hasan and C. L. Kane, Colloquium: Topological insulators, Rev. Mod. Phys. **82**, 3045 (2010).
 - [42] X.-L. Qi and S.-C. Zhang, Topological insulators and superconductors, Rev. Mod. Phys. **83**, 1057 (2011).
 - [43] Y. Tanaka, M. Sato, and N. Nagaosa, Symmetry and topology in superconductors -odd-frequency pairing and edge states-, J. Phys. Soc. Jpn. **81**, 011013 (2012).
 - [44] J. Alicea, New directions in the pursuit of Majorana fermions in solid state systems, Rep. Prog. Phys. **75**, 076501 (2012).
 - [45] Y. Ando and L. Fu, Topological crystalline insulators and topological superconductors: From concepts to materials, Annual Review of Condensed Matter Physics **6**, 361 (2015).
 - [46] M. Sato and S. Fujimoto, Majorana fermions and topology in superconductors, J. Phys. Soc. Jpn. **85**, 072001 (2016).
 - [47] T. Mizushima, Y. Tsutsumi, T. Kawakami, M. Sato, M. Ichioka, and K. Machida, Symmetry-protected topological superfluids and superconductors—from the basics to ^3He —, J. Phys. Soc. Jpn. **85**, 022001 (2016).
 - [48] M. Sato and Y. Ando, Topological superconductors: a review, Rep. Prog. Phys. **80**, 076501 (2017).
 - [49] S. Yonezawa, Bulk topological superconductors, AAPPS Bulletin **26**, 3 (2016).
 - [50] C. Nayak, S. H. Simon, A. Stern, M. Freedman, and S. Das Sarma, Non-abelian anyons and topological quantum computation, Rev. Mod. Phys. **80**, 1083 (2008).
 - [51] Y. S. Hor, A. J. Williams, J. G. Checkelsky, P. Roushan, J. Seo, Q. Xu, H. W. Zandbergen, A. Yazdani, N. P. Ong, and R. J. Cava, Superconductivity in $\text{Cu}_x\text{Bi}_2\text{Se}_3$ and its implications for pairing in the undoped topological insulator, Phys. Rev. Lett. **104**, 057001 (2010).
 - [52] L. Fu and E. Berg, Odd-parity topological superconductors: Theory and application to $\text{Cu}_x\text{Bi}_2\text{Se}_3$, Phys. Rev. Lett. **105**, 097001 (2010).
 - [53] S. Sasaki, M. Kriener, K. Segawa, K. Yada, Y. Tanaka, M. Sato, and Y. Ando, Topological superconductivity in $\text{Cu}_x\text{Bi}_2\text{Se}_3$, Phys. Rev. Lett. **107**, 217001 (2011).
 - [54] S. Sasaki, Z. Ren, A. A. Taskin, K. Segawa, L. Fu, and Y. Ando, Odd-parity pairing and topological superconductivity in a strongly spin-orbit coupled semiconductor, Phys. Rev. Lett. **109**, 217004 (2012).
 - [55] T. Hashimoto, K. Yada, M. Sato, and Y. Tanaka, Surface electronic state of superconducting topological crystalline insulator, Phys. Rev. B **92**, 174527 (2015).
 - [56] L. Fu, Odd-parity topological superconductor with nematic order: Application to $\text{Cu}_x\text{Bi}_2\text{Se}_3$, Phys. Rev. B **90**, 100509(R) (2014).
 - [57] K. Matano, M. Kriener, K. Segawa, Y. Ando, and G.-q.

- Zheng, Spin-rotation symmetry breaking in the superconducting state of $\text{Cu}_x\text{Bi}_2\text{Se}_3$, *Nature Physics* **12**, 852 (2016).
- [58] S. Yonezawa, K. Tajiri, S. Nakata, Y. Nagai, Z. Wang, K. Segawa, Y. Ando, and Y. Maeno, Thermodynamic evidence for nematic superconductivity in $\text{Cu}_x\text{Bi}_2\text{Se}_3$, *Nature Physics* **13**, 123 (2017).
- [59] L. Aggarwal, A. Gaurav, G. S. Thakur, Z. Haque, A. K. Ganguli, and G. Sheet, Unconventional superconductivity at mesoscopic point contacts on the 3D Dirac semimetal Cd_3As_2 , *Nature Materials* **15**, 32–37 (2016).
- [60] H. Wang, H. Wang, H. Liu, H. Lu, W. Yang, S. Jia, X.-J. Liu, X. C. Xie, J. Wei, and J. Wang, Observation of superconductivity induced by a point contact on 3D Dirac semimetal Cd_3As_2 crystals, *Nature Materials* **15**, 38–42 (2016).
- [61] S. Kobayashi and M. Sato, Topological superconductivity in Dirac semimetals, *Phys. Rev. Lett.* **115**, 187001 (2015).
- [62] T. Hashimoto, S. Kobayashi, Y. Tanaka, and M. Sato, Superconductivity in doped Dirac semimetals, *Phys. Rev. B* **94**, 014510 (2016).
- [63] M. Oudah, A. Ikeda, J. N. Hausmann, S. Yonezawa, T. Fukumoto, S. Kobayashi, M. Sato, and Y. Maeno, Superconductivity in the antiperovskite Dirac-metal oxide $\text{Sr}_{3-x}\text{SnO}$, *Nature Communications* **7**, 13617 (2016).
- [64] T. Kawakami, T. Okamura, S. Kobayashi, and M. Sato, Topological crystalline materials of $j = 3/2$ electrons: Antiperovskites, Dirac points, and high winding topological superconductivity, *Phys. Rev. X* **8**, 041026 (2018).
- [65] P. Zhang *et al.*, Multiple topological states in iron-based superconductors, *Nat. Phys.* **15**, 41 (2019).
- [66] T. Kawakami and M. Sato, Topological crystalline superconductivity in Dirac semimetal phase of iron-based superconductors, *Phys. Rev. B* **100**, 094520 (2019).
- [67] W. A. Benalcazar, J. C. Y. Teo, and T. L. Hughes, Classification of two-dimensional topological crystalline superconductors and majorana bound states at disclinations, *Phys. Rev. B* **89**, 224503 (2014).
- [68] M. Sato and S. Fujimoto, Topological phases of noncentrosymmetric superconductors: Edge states, Majorana fermions, and non-Abelian statistics, *Phys. Rev. B* **79**, 094504 (2009).
- [69] S. B. Chung and S.-C. Zhang, Detecting the Majorana fermion surface state of $^3\text{He}-B$ through spin relaxation, *Phys. Rev. Lett.* **103**, 235301 (2009).
- [70] Y. Nagato, S. Higashitani, and K. Nagai, Strong anisotropy in spin susceptibility of superfluid $^3\text{He}-B$ film caused by surface bound states, *J. Phys. Soc. Jpn.* **78**, 123603 (2009).
- [71] R. Shindou, A. Furusaki, and N. Nagaosa, Quantum impurity spin in Majorana edge fermions, *Phys. Rev. B* **82**, 180505(R) (2010).
- [72] T. Mizushima, M. Sato, and K. Machida, Symmetry protected topological order and spin susceptibility in superfluid $^3\text{He}-B$, *Phys. Rev. Lett.* **109**, 165301 (2012).
- [73] Y. Tsutsumi, M. Ishikawa, T. Kawakami, T. Mizushima, M. Sato, M. Ichioka, and K. Machida, UPt_3 as a topological crystalline superconductor, *J. Phys. Soc. Jpn.* **82**, 113707 (2013).
- [74] Y. Xiong, A. Yamakage, S. Kobayashi, M. Sato, and Y. Tanaka, Anisotropic magnetic responses of topological crystalline superconductors, *Crystals* **7**, 58 (2017).
- [75] Y. Volpez, D. Loss, and J. Klinovaja, Second-order topological superconductivity in π -junction Rashba layers, *Phys. Rev. Lett.* **122**, 126402 (2019).
- [76] S. Kobayashi, A. Yamakage, Y. Tanaka, and M. Sato, Majorana multipole response of topological superconductors, *Phys. Rev. Lett.* **123**, 097002 (2019).
- [77] Y. Yamazaki, S. Kobayashi, and A. Yamakage, Magnetic response of Majorana kramers pairs protected by \mathbb{Z}_2 invariants, *J. Phys. Soc. Jpn.* **89**, 043703 (2020).
- [78] K. Plekhanov, N. Müller, Y. Volpez, D. M. Kennes, H. Schoeller, D. Loss, and J. Klinovaja, Quadrupole spin polarization as signature of second-order topological superconductors, *Phys. Rev. B* **103**, L041401 (2021).
- [79] Y. Yamazaki, S. Kobayashi, and A. Yamakage, Magnetic response of Majorana kramers pairs with an order-two symmetry, *Phys. Rev. B* **103**, 094508 (2021).
- [80] B. Kayser and A. S. Goldhaber, CPT and CP properties of Majorana particles, and the consequences, *Phys. Rev. D* **28**, 2341 (1983).
- [81] E. E. Radescu, On the electromagnetic properties of Majorana fermions, *Phys. Rev. D* **32**, 1266 (1985).
- [82] F. Boudjema, C. Hamzaoui, V. Rahal, and H. C. Ren, Electromagnetic properties of generalized Majorana particles, *Phys. Rev. Lett.* **62**, 852 (1989).
- [83] S. A. Yang, H. Pan, and F. Zhang, Dirac and Weyl superconductors in three dimensions, *Phys. Rev. Lett.* **113**, 046401 (2014).
- [84] T. Mizushima, Odd-frequency pairing and ising spin susceptibility in time-reversal-invariant superfluids and superconductors, *Phys. Rev. B* **90**, 184506 (2014).
- [85] S. Kobayashi, K. Shiozaki, Y. Tanaka, and M. Sato, Topological Blount's theorem of odd-parity superconductors, *Phys. Rev. B* **90**, 024516 (2014).
- [86] S. Kobayashi, S. Sumita, Y. Yanase, and M. Sato, Symmetry-protected line nodes and Majorana flat bands in nodal crystalline superconductors, *Phys. Rev. B* **97**, 180504(R) (2018).
- [87] H. Hu, F. Zhang, and C. Zhang, Majorana doublets, flat bands, and Dirac nodes in s -wave superfluids, *Phys. Rev. Lett.* **121**, 185302 (2018).
- [88] G. Goll, M. Marz, A. Hamann, T. Tomanic, K. Grube, T. Yoshino, and T. Takabatake, Thermodynamic and transport properties of the non-centrosymmetric superconductor LaBiPt , *Physica B: Condensed Matter* **403**, 1065 (2008).
- [89] N. P. Butch, P. Syers, K. Kirshenbaum, A. P. Hope, and J. Paglione, Superconductivity in the topological semimetal YPtBi , *Phys. Rev. B* **84**, 220504(R) (2011).
- [90] F. F. Tafti, T. Fujii, A. Juneau-Fecteau, S. René de Cotret, N. Doiron-Leyraud, A. Asamitsu, and L. Taillefer, Superconductivity in the noncentrosymmetric half-Heusler compound LuPtBi : A candidate for topological superconductivity, *Phys. Rev. B* **87**, 184504 (2013).
- [91] G. Xu, W. Wang, X. Zhang, Y. Du, E. Liu, S. Wang, G. Wu, Z. Liu, and X. X. Zhang, Weak antilocalization effect and noncentrosymmetric superconductivity in a topologically nontrivial semimetal LuPdBi , *Scientific Reports* **4**, 5709 (2014).
- [92] T. V. Bay, T. Naka, Y. K. Huang, and A. de Visser, Superconductivity in noncentrosymmetric YPtBi under pressure, *Phys. Rev. B* **86**, 064515 (2012).
- [93] P. M. R. Brydon, L. Wang, M. Weinert, and D. F. Agterberg, Pairing of $j = 3/2$ fermions in Half-Heusler superconductors, *Phys. Rev. Lett.* **116**, 177001 (2016).

- [94] H. Kim, K. Wang, Y. Nakajima, R. Hu, S. Ziemak, P. Syers, L. Wang, H. Hodovanets, J. D. Denlinger, P. M. R. Brydon, D. F. Agterberg, M. A. Tanatar, R. Prozorov, and J. Paglione, Beyond triplet: Unconventional superconductivity in a spin-3/2 topological semimetal, *Science Advances* **4**, eaao4513 (2018).
- [95] A. Daido, T. Yoshida, and Y. Yanase, \mathbb{Z}_4 topological superconductivity in UCoGe, *Phys. Rev. Lett.* **122**, 227001 (2019).
- [96] T. Yoshida, A. Daido, N. Kawakami, and Y. Yanase, Efficient method to compute \mathbb{Z}_4 indices with glide symmetry and applications to the Möbius materials CeNiSn and UCoGe, *Phys. Rev. B* **99**, 235105 (2019).
- [97] S. Jeon, Y. Xie, J. Li, Z. Wang, B. A. Bernevig, and A. Yazdani, Distinguishing a Majorana zero mode using spin-resolved measurements, *Science* **358**, 772 (2017).
- [98] L. Cornils, A. Kamlapure, L. Zhou, S. Pradhan, A. A. Khajetoorians, J. Fransson, J. Wiebe, and R. Wiesendanger, Spin-resolved spectroscopy of the Yu-Shiba-Rusinov states of individual atoms, *Phys. Rev. Lett.* **119**, 197002 (2017).
- [99] R. Nakai and K. Nomura, Disorder effects on thermal transport on the surface of topological superconductors by the self-consistent Born approximation, *Phys. Rev. B* **89**, 064503 (2014).
- [100] H.-Y. Xie, Y.-Z. Chou, and M. S. Foster, Surface transport coefficients for three-dimensional topological superconductors, *Phys. Rev. B* **91**, 024203 (2015).
- [101] N. V. Gnezdilov, M. Diez, M. J. Pacholski, and C. W. J. Beenakker, Wiedemann-Franz-type relation between shot noise and thermal conduction of Majorana surface states in a three-dimensional topological superconductor, *Phys. Rev. B* **94**, 115415 (2016).
- [102] P. G. Grinevich and G. E. Volovik, Topology of gap nodes in superfluid ^3He : π_4 homotopy group for $^3\text{He}-B$ disclination, *Journal of Low Temperature Physics* **72**, 371 (1988).
- [103] M. Sato, Topological odd-parity superconductors, *Phys. Rev. B* **81**, 220504(R) (2010).
- [104] C. J. Bradley and A. P. Cracknell, *The Mathematical Theory of Symmetry in Solids* (Oxford University Press, New York, 2003).
- [105] E. P. Wigner, *Group Theory and its Application to the Quantum Mechanics of Atomic Spectra* (Academic Press, New York, 1959).
- [106] C. Herring, Effect of time-reversal symmetry on energy bands of crystals, *Phys. Rev.* **52**, 361 (1937).
- [107] T. Inui, Y. Tanabe, and Y. Onodera, *Group theory and its applications in physics*, Springer Series in Solid-State Sciences, Vol. 78 (Springer-Verlag Berlin Heidelberg, Berlin, Heidelberg, 1990).
- [108] K. Shiozaki, M. Sato, and K. Gomi, Atiyah-Hirzebruch spectral sequence in band topology: General formalism and topological invariants for 230 space groups, (2018), arXiv:1802.06694 [cond-mat.str-el].
- [109] S. Sumita, T. Nomoto, K. Shiozaki, and Y. Yanase, Classification of topological crystalline superconducting nodes on high-symmetry lines: Point nodes, line nodes, and Bogoliubov Fermi surfaces, *Phys. Rev. B* **99**, 134513 (2019).
- [110] L. Elcoro, B. Bradlyn, Z. Wang, M. G. Vergniory, J. Cano, C. Felser, B. A. Bernevig, D. Orobengoa, G. de la Flor, and M. I. Aroyo, Double crystallographic groups and their representations on the Bilbao Crystallographic Server, *Journal of Applied Crystallography* **50**, 1457 (2017).
- [111] Here $g(\mathbf{B})$ and \hat{O} can be multi-component, and the summation of the multi-component indices are implicit.
- [112] Q.-Z. Wang and C.-X. Liu, Topological nonsymmorphic crystalline superconductors, *Phys. Rev. B* **93**, 020505(R) (2016).
- [113] E. Witten and D. Olive, Supersymmetry algebras that include topological charges, *Physics Letters B* **78**, 97 (1978).
- [114] Y. Tanaka and S. Kashiwaya, Theory of tunneling spectroscopy of d -wave superconductors, *Phys. Rev. Lett.* **74**, 3451 (1995).
- [115] Y. Tanaka, Y. Tanuma, K. Kuroki, and S. Kashiwaya, Theory of magnetotunneling spectroscopy in spin triplet p -wave superconductors, *J. Phys. Soc. Jpn.* **71**, 2102 (2002).
- [116] Y. Tanuma, K. Kuroki, Y. Tanaka, R. Arita, S. Kashiwaya, and H. Aoki, Determination of pairing symmetry from magnetotunneling spectroscopy: A case study for quasi-one-dimensional organic superconductors, *Phys. Rev. B* **66**, 094507 (2002).
- [117] Y. Tanaka, T. Yokoyama, A. V. Balatsky, and N. Nagaosa, Theory of topological spin current in non-centrosymmetric superconductors, *Phys. Rev. B* **79**, 060505(R) (2009).
- [118] S. Tamura, S. Kobayashi, L. Bo, and Y. Tanaka, Theory of surface andreev bound states and tunneling spectroscopy in three-dimensional chiral superconductors, *Phys. Rev. B* **95**, 104511 (2017).
- [119] L. Chiroli and F. Guinea, Magnetic tilting and emergent Majorana spin connection in topological superconductors, *Phys. Rev. B* **98**, 094515 (2018).
- [120] E. Dumitrescu, J. D. Sau, and S. Tewari, Magnetic field response and chiral symmetry of time-reversal-invariant topological superconductors, *Phys. Rev. B* **90**, 245438 (2014).
- [121] B. Lu, K. Yada, M. Sato, and Y. Tanaka, Crossed surface flat bands of Weyl semimetal superconductors, *Phys. Rev. Lett.* **114**, 096804 (2015).